Nanotribology and nanomechanics of AFM probe-based data recording technology

2008 J. Phys.: Condens. Matter 20 365207

(http://iopscience.iop.org/0953-8984/20/36/365207)

J. Phys.: Condens. Matter **20** (2008) 365207 (34pp) doi:10.1088/0953-8984/20/36/365207

Nanotribology and nanomechanics of AFM probe-based data recording technology

Bharat Bhushan[1], **Kwang Joo Kwak and Manuel Palacio**

Nanoprobe Laboratory for Bio- and Nanotechnology and Biomimetics, Ohio State University, 201 West 19th Avenue, Columbus, OH 43210-1142, USA

E-mail: bhushan.2@osu.edu

Received 16 June 2008, in final form 24 July 2008
Published 14 August 2008
Online at stacks.iop.org/JPhysCM/20/365207

Abstract

With the advent of scanning probe microscopes, probe-based data recording technologies are being developed for ultrahigh areal density recording, where the probe tip is expected to be scanned at velocities up to 100 mm s^{-1}. In one technique, a conductive atomic force microscope (AFM) tip is scanned over a phase change chalcogenide medium and phase change is accomplished by applying either a high or low magnitude of current which heats the interface. Another technique is ferroelectric data storage, where a conducting AFM tip is scanned over a lead zirconate titanate (PZT) film, a ferroelectric material. Ferroelectric domains can be polarized by applying short voltage pulses between the AFM tip and the bottom electrode layer that exceed the coercive field of the PZT film, resulting in nonvolatile changes in the electronic properties. Tip wear is a serious concern in both data storage methods. The understanding and improvement of tip wear, particularly at the high velocities needed and at high interface temperatures for high data rate recording, is critical to the commercialization of these data storage technologies.

This paper presents a review of nanotribological and nanomechanical studies on the materials used in phase change and ferroelectric probe-based recording. Although this work is aimed at probe-based data recording, it is also relevant to the development of robust AFM probes and to the study of nanocontacts in general.

1. Introduction

Nonvolatile digital data storage systems include electrically addressed systems such as flash memories and mechanically addressed systems such as magnetic tapes, optical disks and magnetic hard disks (Bhushan 1996, Fazio 2004). The latter have much higher storage capacity and relies on the physical movement of the recording medium or a reading head. Recently, both flash memories and miniature disk drives have begun to replace each other, mostly in portable but also in some fixed devices which require a relatively low storage capacity (Coughlin and Handy 2006). Both magnetic hard disks and flash memories continue to provide significant technical advances in storage capacity as well as performance and reliability. With magnetic recording, most devices use longitudinal recording where the magnetization prefers to lie in the plane of the recording medium. Perpendicular recording, which is also used, typically exhibits higher limiting areal densities than longitudinal: for example, these densities are projected to be 500 and 100 Gb in^{-2} at SNR of 20 dB, respectively (Bertram and Williams 2000, Richter 2007). Heat-assisted magnetic recording (HAMR) and recording on bit-patterned media have been identified as future technologies to extend magnetic recording. HAMR recording makes the recording device more complicated. The head structure needs to be augmented by a laser with a near-field optical system to accomplish the heating (Rottmayer *et al* 2006). For the bit-patterned media, media need to have nanopatterns. It is to be noted that the head–medium spacing is one of the important factors for the drastic increase in areal density (Bhushan 1996).

With the advent of scanning probe microscopes (SPM), probe-based recording technologies are being developed for

[1] Author to whom any correspondence should be addressed.

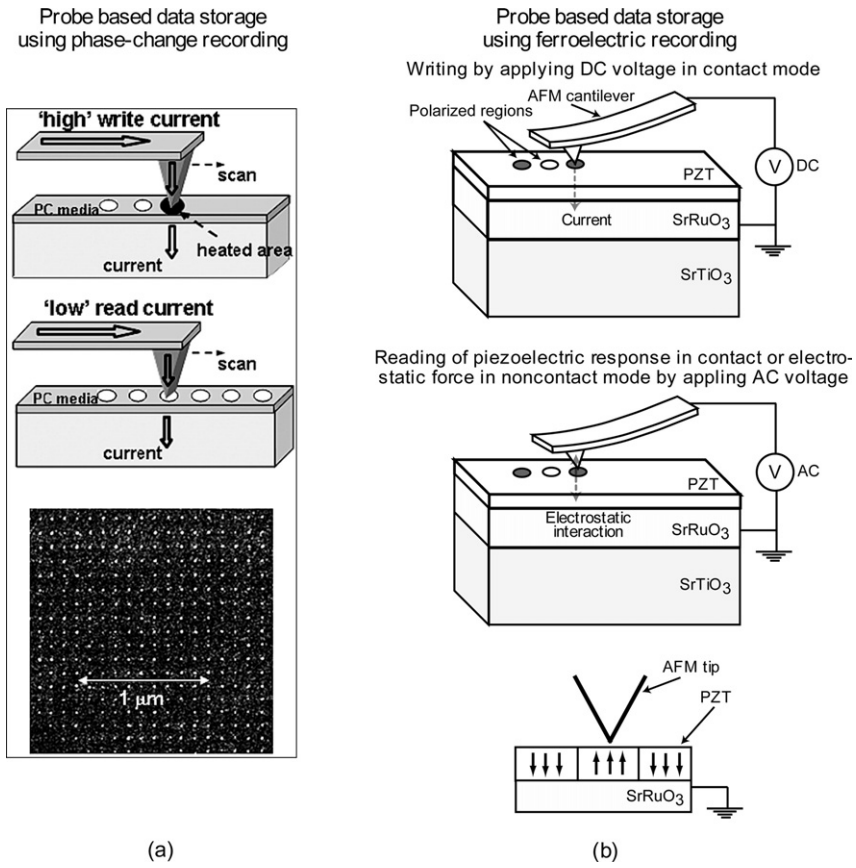

Figure 1. (a) Schematic of the electrical probe storage system using phase change media (Wright *et al* 2006). (b) Schematics of the AFM probe-based storage system using ferroelectric media (Bhushan and Kwak 2008b).

ultrahigh areal density. Many approaches using probe-based techniques have been brought forward (Cooper *et al* 1999, Vettiger *et al* 1999, Shin *et al* 2000, Bhushan and Kwak 2007a, 2008b, Kwak and Bhushan 2008). Various recording techniques using thermomechanical (Mamin and Rugar 1992, Vettiger *et al* 1999), phase change (Kado and Tohda 1995, Gidon *et al* 2004, Wright *et al* 2006), magnetic (Ohkubo *et al* 1991), thermomagnetic (Nakamura *et al* 1995, Zhang *et al* 2002), optical (Betzig *et al* 1992), electrical (Barrett and Quate 1991) and ferroelectric (Franke *et al* 1994, Ahn *et al* 1997) methods have been demonstrated. A probe-based storage device with an atomic force microscope (AFM) tip has the potential to achieve ultrahigh areal densities of the order of several Tb in^{-2} or higher. Another great advantage of a probe-based recording technique is the use of a multiple probe array for high data rate. The IBM group has developed a technology which uses an array of 1024 silicon cantilevers (Millipede) for thermomechanical recording and playback on an about 40 nm thick polymer with a harder Si substrate (Vettiger *et al* 1999). The cantilevers consist of integrated heaters with tips of nanoscale dimensions. The tip, heated to about 400 °C, is brought into contact with the polymer for recording. Reading is done using the heated cantilever, originally used for recording, as a thermal readback sensor by exploiting its temperature-dependent resistance. Wear of the heated tip is an issue.

A second technique using a probe-based recording system is phase change memory (PCM) (Kado and Tohda 1995, Gidon *et al* 2004, Wright *et al* 2006), which has the potential for dramatic progress in memory devices (Maimon *et al* 2001, Strand 2005). A schematic of the electrical probe storage system using phase change media is shown in figure 1(a) (Wright *et al* 2006). The pioneering work of Stanford Ovshinsky in the 1960s on switching (Ovshinsky 1968) and memory effects in chalcogenide alloys motivated the field of amorphous semiconductors. Chips based on ovonic unified memory (OUM^{TM}) storage generate different levels of high and low resistance on a glassy material, which represent 1 and 0 states in binary recording. An OUM nonvolatile memory cell uses a horizontal strip of chalcogenide—a type of electrically conductive glass material—connected to an electrode, already used in rewritable CD technology. When a high current is applied through the electrode probe, the chalcogenide medium is heated to more than 630 °C, creating a region of amorphous glass with high resistance. When a lower current is applied, it heats up to a temperature less than 630 °C and then cools to a crystalline state with lower resistance. In the reading mode, a low level current is passed through the tip to the medium to sense the high resistance amorphous state or the low resistance crystalline state. The probe needs to be electrically conductive, and a high-conductivity Pt coating can be deposited on the silicon probe. For a fast data transfer rate, the cantilever array needs to be moved at high velocities, of the order of 100 mm s^{-1}. Friction and wear at high velocities, high loads and in high temperature conditions are

major impediments to this technology (Bhushan and Kwak 2007a). A significant concern is the durability of the probe tips during the recording process at temperatures as high as 630 °C during sliding contact at relatively high velocities of the order of tens of mm s^{-1}. Bhushan and Kwak (2007a, 2007b, 2008a) investigated the velocity and temperature dependence of probe tip wear during sliding with diamond-like carbon (DLC) films. DLC is used to protect the phase change chalcogenide medium from wear. Possible wear mechanisms of the probe tip–sample contacts include adhesive wear, abrasive wear and low cycle fatigue (Su *et al* 2003, Tao and Bhushan 2006a, 2006b), and these mechanisms in combination with tribochemical reactions are important at high velocities. Specifically, for phase change data recording, Bhushan and Kwak (2007a, 2007b) found that wear occurs by adhesive, abrasive and tribochemical wear modes. The increase in wear with the logarithm of velocity at low sliding velocities is associated with thermally activated atomic-scale stick–slip. They also reported temperature dependence of wear, i.e. increasing the test temperature to 80 °C leads to an increase in the wear rate compared to ambient.

A third technique is ferroelectric memory, which is used as ferroelectric random access memory (FeRAM) in an electrically addressed storage system (Setter *et al* 2006). In a FeRAM, the dielectric structure includes ferroelectric material, typically lead zirconate titanate (PZT). When an external electric field is applied across the ferroelectric medium, positive or negative charges will be displaced from their original position—a concept that is characterized by polarization. In a ferroelectric material, there is a spontaneous polarization—a displacement that is inherent to the crystal structure of the material. The direction of this polarization can be reversed or reoriented by applying an electric field. Thus, the application of an electric field can be used to change the polarization direction of the medium; typically binary 1 and 0 states are stored as one of two possible electric polarizations in each data storage cell.

There are a number of alternative approaches on the basis of ferroelectric materials for nonvolatile data storage, such as ferroelectric field effect transistors (Arimoto and Ishiwara 2004), ferroelectric resistive-based data storage (Blom *et al* 1994) and ferroelectric tunnel junctions (Zhuravlev *et al* 2005). An alternative ferroelectric data storage method is a mechanically addressed storage system which uses a probe-based recording technique (Franke *et al* 1994, Hidaka *et al* 1996, Ahn *et al* 1997, Shin *et al* 2002). The schematic of domain writing and reading in ferroelectric films is shown in figure 1(b) (Bhushan and Kwak 2008b). For example, a conductive AFM tip is placed in contact with a storage medium consisting of $SrTiO_3$ (STO), coated with a $PbZr_{0.52}Ti_{0.48}O_3/SrRuO_3$ (PZT/SRO) double layer (Franke *et al* 1994, Ahn *et al* 1997). The SRO serves as the bottom electrode and PZT represents the ferroelectric film. Ferroelectric domains can be polarized by applying short voltage pulses (∼10 V, ∼100 μs) between the AFM tip and the SRO electrode that exceed the coercive field of the PZT layer, resulting in local, nonvolatile changes in the electronic properties of the underlying film. In epitaxial *c*-axis-oriented PZT films, the polarization vector can be parallel or antiparallel to the *c* axis. An example for a series of ferroelectric bits on the domain radius vs. pulse duration width has been achieved by Tybell *et al* (2002). The activation energy increases significantly from 50 to 130 MV m^{-1} as the film thickness is reduced from 81 to 29 nm. In principle, thinner PZT films should result in smaller domains and higher storage densities. It should be noted that the temperature rise during recording should be of the order of 80 °C, which alleviates wear issues. Furthermore, the tip does not need to be in contact with the medium during readback.

There are two different methods for reading out the polarization state in ferroelectric thin films. Imaging of ferroelectric domains in thin films makes use of the basic properties of ferroelectrics, namely their piezoelectric behavior and the presence of surface charge. A static surface charge, proportional to the normal component of polarization, can be detected by electrostatic force microscopy (EFM), when the microscope is operating in the noncontact mode, as shown in figure 1(b) (Saurenbach and Terris 1990). A similar detection mechanism is demonstrated for previously written ferroelectric domains on a PZT/Nb-doped $SrTiO_3$ by Ahn *et al* (1997). In the noncontact regime, these voltage modulation techniques, such as Kelvin probe force microscopy (KPFM), are sensitive to voltage derivation of the force (Martin *et al* 1988, Nonnenmacher *et al* 1991). In the second method, an AFM is operated in the contact mode and piezoresponse force is measured by applying an AC voltage; the method is called piezoresponse force microscopy (PFM) (Guthner and Dransfeld 1992, Franke *et al* 1994, Gruverman *et al* 1996, Roelofs *et al* 2000). By monitoring the piezoelectric vibration of the ferroelectric film caused by an external AC voltage, the domain structure can be visualized in the AFM piezoresponse mode when the probing tip is in contact with the film surface (Gruverman *et al* 1996). In this piezoresponse mode, the voltage is applied through the probe tip, which is used as a movable top electrode. The modulated deflection signal from the cantilever, which oscillates together with the thin film due to tip–sample contact, is detected using the lock-in amplifier, as in the case of noncontact detection.

Considering the fidelity of AFM probe-based data storage, it is noted that the application of a voltage pulse to the PZT film results in a change of its thickness. A degradation phenomenon to be considered in connection with the reliability problem is ferroelectric fatigue, or the decrease of switchable polarization with repeated polarization reversal (Mihara *et al* 1994). The understanding and the improvement of this polarization fatigue might be the key to the commercialization of high density ferroelectric memories. Another important reliability issue to be considered in probe-based data storage is tip wear with tip–sample contact (Bhushan and Kwak 2007a). Under typical PFM operating conditions, the total force acting on a tip, F, is equal to $F_o + F_{el}$, where $F_o (= kd_o)$ is an elastic force exerted by a cantilever of spring constant k at set point deflection, d_o, and F_{el} is an electrostatic force (Kalinin and Bonnell 2002). When a normal force is much larger than the electrostatic force, $F_{el} \ll F_o$, an average stress below a tip is of the order of 1.3 GPa for an assumed contact radius of ∼5 nm,

Table 1. Details of noble-metal-coated probes.

	Tip		
Noble metal	Stiffness (N m^{-1}) and initial 2D tip radius (nm)	Thickness of metal films (nm)	PZT flat sample
Pt	∼2 N m^{-1}, 74 nm (CSC21, MikroMasch)	185 nm/15 nm Pt/Cr (sputter deposition)	15 nm/50 nm $PbZr_{0.2}Ti_{0.8}O_3/SrRuO_3$ film on 0.5 mm *c*-axis $SrTiO_3$ (pulsed laser deposition)
Au–Ni	∼2.8 N m^{-1}, 65 nm Au–Ni (PPP-FM, Nanosensors)	65 nm/10 nm Au–Ni/Cr (sputter deposition with Au–Ni alloy, and sputtering with Cr target, respectively)	
Pt–Ir	∼2.8 N m^{-1}, 53 nm Pt–Ir (PPP-EFM, Nanosensors)	25 nm/3 nm Pt–Ir/Cr (sputter deposition)	
Pt–Ni	∼2.8 N m^{-1}, 61 nm Pt–Ni (PPP-FM, Nanosensors)	95 nm/10 nm Pt–Ni/Ni (Co-sputtering with separate Pt and Ni targets, and sputtering with Ni target, respectively)	

corresponding to a normal force of ∼100 nN (Bhushan and Kwak 2008b).

In order to achieve high wear resistance and a long lifetime, a high surface hardness of a noble-metal-coated tip is essential. However, a noble-metal-deposited tip surface has a lower hardness than that of typically used Si tips. The selection of a top metal layer on the tip depends on material hardness, electrical conductivity, melting point and deposition processing difficulty. The failure mechanism is particularly severe for soft metals such as pure Au. An alloy such as Au–Ni_5 (gold with an alloying addition of 5% nickel), a hard contact material used in relays, can be used in the selection of the top metal layer. A wear-resistant tip including an alloy of platinum, iridium and tungsten has been introduced for spark plugs by AlliedSignal Inc. (Kozlov *et al* 2000). By adding a small amount of tungsten to a platinum–iridium alloy, the wear resistance of the spark plug is improved. Several metals that could potentially provide some of the desirable properties are listed in table 1 (Bhushan and Kwak 2008b). It is noted that the metal properties can vary significantly based on the deposition condition of the materials. It is well known that the resistivity of a sputtered metal film could be much higher than its bulk resistivity (Rooney *et al* 1990, Conoci *et al* 2006). The tip wear mechanism on the nanoscale is not well understood, especially with various top metal layers on the probe tip. Single or multiple mechanisms can be responsible for tip wear dependent on the operating conditions. For example, Bhushan and Kwak (2008b, 2008c) and Kwak and Bhushan (2008) found that adhesive and abrasive wear are the main mechanisms during wear of various noble-metal-coated AFM tips sliding on PZT. They also reported the dependence of tip wear on sliding velocity. Wear increases as the logarithm of velocity in the lower velocity range, which is based on the thermally activated stick–slip mechanism. At higher velocities, the predominant wear mechanisms are adhesive and impact wear. Wear was found to increase with the temperature, where a significant difference in the wear rate was observed between experiments carried out at 20 and 80 °C (Bhushan and Kwak 2008b, 2008c, Kwak and Bhushan 2008). In addition, wear was found to increase as a function of humidity, based on experiments conducted at 5–80% relative humidity (RH) range (Bhushan and Kwak 2008c).

The commercial AFM probes with noble metal coatings have primarily been optimized for electrical properties. Nanomechanical properties of the coatings and substrate materials were reported by (Palacio and Bhushan 2008a, 2008b). The knowledge of hardness, elastic modulus and scratch behavior is important in understanding the wear behavior of the probe tips used.

The purpose of this paper is to provide an overview of the nanotribological and nanomechanical properties of materials used in probe-based recording based on recently published work. Section 2 describes the experimental methods which have been used for characterizing the tip and for performing adhesion and friction measurements with AFM. Section 3 describes nanotribological studies on phase change chalcogenide technology, which uses diamond-like carbon (DLC) as the wear-protection overcoat. Section 4 describes nanotribological and nanomechanical studies on ferroelectric data recording technology, conducted on the lead zirconate titanate (PZT) substrate and the AFM tips coated with a noble metal, noble metal alloys and a silicide. Although this paper is on probe-based recording technology, the findings are also relevant to the development of AFM probes and to nanocontacts in general.

2. Experimental techniques

Tip shape characterization and friction and wear measurement techniques used in the studies included in this paper are reviewed below.

2.1. Tip shape characterization

A silicon TGT1 grating sample (NT-MDT, Moscow, Russia) was used for probe tip characterization (Tao and Bhushan 2006a, 2006b, Bhushan and Kwak 2007a, 2008b). As shown in figure 2(a), the grating sample has an array of sharp tips on the surface (Bhushan and Kwak 2007a, 2008b). The tips are arranged on each corner and at the center of a 3 × 3 μm^2 square area. The height of each tip is 0.4 μm. The tip angle is about 30° and the radius of the tip is less than 10 nm. SPIP^{TM} software (Scanning Probe Image Processor, Image

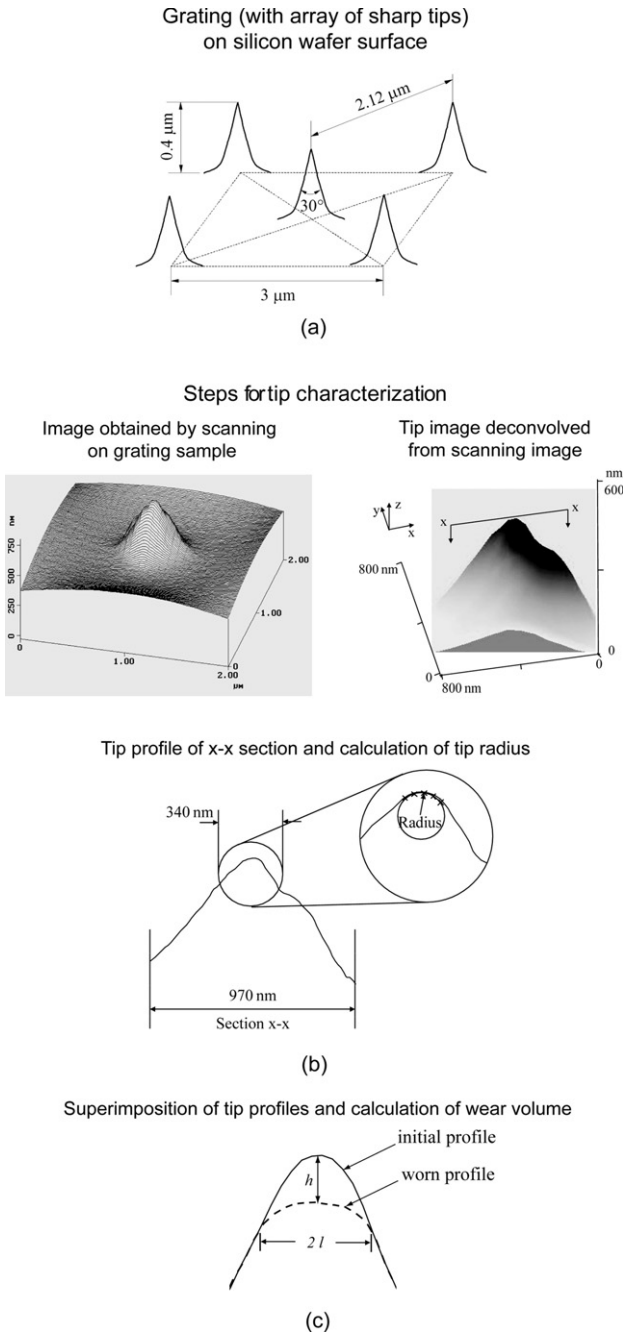

Figure 2. (a) A schematic of a grating (with an array of sharp tips) on a silicon wafer surface, (b) illustration of tip characterization and calculation of tip radius; top left is an image obtained by scanning on a grating sample, top right is the tip image deconvoluted from a scanned image, bottom is the tip profile of x–x section and calculation of tip radius, and (c) illustration of calculation of the wear volume (Bhushan and Kwak 2007a, 2008b).

Metrology A/S, Denmark) was used to characterize the tip and evaluate the tip radius. The processing procedure is illustrated in figure 2(b) (Bhushan and Kwak 2007a, 2008b). The image was first obtained in tapping mode by scanning the tip on the TGT1 grating sample in a direction perpendicular to the long axis of the cantilever beam. Scanning was performed on a 2×2 μm^2 scan area with a velocity of 1 μm s^{-1} in the fast scan direction. The 3D surface of the tip was generated with 970 nm $\times$ 970 nm size (63 points $\times$ 63 points) using the blind tip reconstruction algorithm from the scanned image (Villarrubia 1994). Even if the probe tip has an asymmetric shape, a simple semicircle could be more easily fitted on the 2D tip profile than a hemisphere to a 3D surface; therefore, the 2D tip radius was calculated. The algorithm was used to generate a 2D profile from the tip surface in the scanning direction at the highest location. Tip radius was calculated for a profile with several tens of nm in length by a circle fitted with at least five data points (15.4 nm apart) using the SPIP software.

The initial 2D tip radius is an important factor in determining the wear rate. The initial radius also depends on the thickness of the coated-metal films. The deposition condition of the metal films, such as deposition angle and deposition rate, affects the initial shape and 2D radius. The tip radius and probe shape strongly affect the contact area between the tip and the film during the wear experiments. The larger contact area tends to increase wear volume in sliding on the film. After the coating is removed, the Si tip substrate is exposed, and then the wear volume increases rapidly with an increase in the sliding distance.

2.2. *Friction and wear measurements*

Friction and wear tests were conducted using a Dimension 3000 AFM (Digital Instruments). Measurements were performed in ambient environment (22 $\pm$ 1 °C, 50 $\pm$ 5% relative humidity) unless specified. The friction force experiments were carried out by scanning the sample along an axis perpendicular to the long axis of the cantilever, at a scan velocity of 1 μm s^{-1} using a scan rate of 0.5 Hz at normal loads ranging from 1 to 80 nN (Bhushan and Kwak 2007a, 2008b). The effect of z-piezo movement on the normal load due to thermal drift was monitored and was found to be within 10%. The measured friction force was plotted as a function of normal load. The data could be fitted with a straight line which suggests that friction force is proportional to normal load. The coefficient of friction was obtained by calculating the slope of the line (Ruan and Bhushan 1994, Bhushan 2002, 2008).

For wear experiments, a high velocity piezo stage, developed by Tao and Bhushan (2006c), was used at 10 mm s^{-1} (frequency = 10 Hz) and 100 mm s^{-1} (frequency = 50 Hz) sliding velocities (Bhushan and Kwak 2007a, 2008b). The system includes a custom calibrated piezo stage or a piezo ultrasonic linear drive (M663.465, Physik Instrumente, GmbH & Co. KG, Karlsruhe, Germany), a stage controller (C865, Physik Instrumente) and a self-designed software application for operation control. A sliding velocity of 10 mm s^{-1} was used for a maximum sliding distance of 100 m. A higher velocity at 100 mm s^{-1} was used for a total sliding distance of 300 m to reduce the test duration. The length of a single line scan for the line profile mode was 500 μm and 1000 μm for average sliding velocities of 10 and 100 mm s^{-1}, respectively. For sliding distances of 1, 3, 10, 30 and 100 m, sliding duration was 1×10^2, 3×10^2, 1×10^3, 3×10^3 and 1×10^4 s at sliding velocities of 10 mm s^{-1}, respectively. For the remaining 200 m distance, sliding duration was 2×10^3 s at sliding velocities of 100 mm s^{-1}. Scan direction was parallel to the long axis of the cantilever beam.

For wear measurements, each probe was first scanned on the grating sample in tapping mode to obtain the initial image for tip characterization (Tao and Bhushan 2006a, Bhushan and Kwak 2007a, 2008b). After scanning on the grating sample, the tip was slid on a film sample in contact mode. After the wear test, the probe was scanned again on the grating sample to obtain an image for tip characterization. The wear volume was calculated from the tip profiles before and after the wear experiment. In order to calculate the wear volume, the profile after sliding was manually superimposed on the original profile so that they coincide (largely) with each other, see figure 2(c) (Bhushan and Kwak 2007a, 2008b). The worn region was assumed to be cone-shaped. The worn height (h) of the cone was the distance between the tops of the original and worn tips, and $2l$ was the width of the base of the worn region. The wear volume was calculated as $V = \pi l^2 h/3$.

3. Nanotribological characterization—phase change recording technology

Phase change recording technology uses an AFM cantilever array and a phase change memory medium such as chalcogenide (Wright *et al* 2006) and has a potential of storing tens of Gb per chip. For wear protection of the phase change medium, a diamond-like carbon (DLC) coating is deposited on the recording layer/silicon substrate (Bhushan 1999a). From nanoindentation measurements, DLC has hardness and elastic modulus ranging from 15–24 GPa and 140–280 GPa, respectively (Bhushan 1999a, 2008). The mechanical properties of DLC makes wear of the noble metal coating in the probe tip inevitable. Lubrication of either the tip or DLC surface reduces the extent of wear and makes this probe-based technology feasible.

The liquid lubricants that can be physically and chemically bonded to the silicon and DLC surface are attractive candidates for tip and medium coating. Chemically bonded liquid lubricants of perfluoropolyethers (PFPEs) are widely used in the construction of magnetic rigid disks and metal-evaporated tapes (Bhushan 1996, 2008). Z-TETRAOL 2000 (Solvay Solexis Inc.) (to be referred to as Z-TETRAOL) is a derivative of PFPEs with a double hydroxyl group at each end of the polymer chain. Tao and Bhushan (2005) reported that Z-TETRAOL applied on a silicon wafer surface showed better durability at various humidity levels as compared to the conventional PFPE lubricant Z-DOL (Solvay Solexis Inc.) with one hydroxyl group at each end.

In this section, nanotribological studies conducted by Bhushan and Kwak (2007a, 2007b, 2008a) on the sliding of Pt-coated Si tips on a DLC-coated phase change medium is reviewed. These studies focus on the role of load, sliding velocity, distance and temperature on the tip wear mechanism.

3.1. Experimental samples

In the studies reviewed in this section, triangular etched single-crystal silicon cantilevers with conical probe tips (CSC21, MikroMasch) coated with 185 nm/15 nm thick Pt/Cr using sputter deposition were used, figure 3 (left) (Bhushan and Kwak 2007a). The length and width of both cantilever legs were 110 μm and 40 μm, respectively. The nominal spring constants of the cantilever and tip radius are 2 N m^{-1} and 10 nm before coating (provided by the manufacturer), respectively.

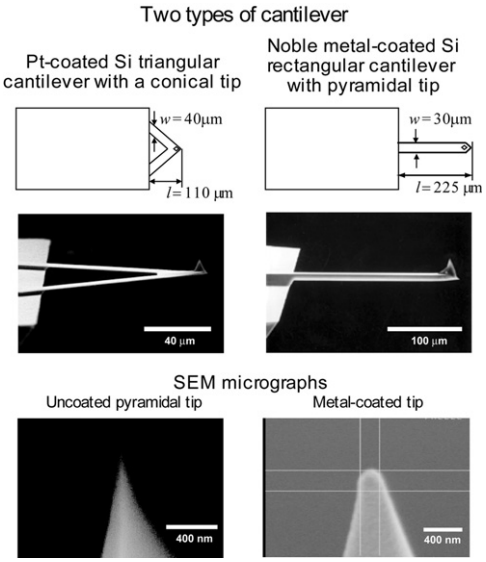

Figure 3. Schematic (top) and photographs (middle) of a Pt-coated Si triangular cantilever with a conical tip, and a noble-metal-coated Si rectangular cantilever with pyramidal tip, along with high magnification SEM micrographs (bottom) of uncoated and metal-coated tips (Bhushan and Kwak 2008b).

Diamond-like carbon (DLC) film was used for coating silicon disks with chalcogenide ($Ge_2Sb_2Te_5$) deposited by sputtering (Bhushan and Kwak 2007a). Z-TETRAOL (Solvay Solexis) was used to lubricate the DLC film. A film of Z-TETRAOL was deposited on the DLC surfaces by the dip coating technique (Tao and Bhushan 2006a). Partially bonded films (Z-TETRAOL) were obtained by heating at 150 °C for 30 min without further treatment. The film thickness of Z-TETRAOL was 3 nm and its mobile fraction was about 0.8 nm thick (Tao and Bhushan 2006a). For this technology, any coating applied on the medium should have some electrical conductivity. The electrical resistivity of PFPE (Z-DOL) is 3.9×10^{13} Ω cm, which may be adequate.

3.2. Unlubricated and Z-TETRAOL-lubricated DLC disks

Figure 4(a) shows the tip profiles after 1 m sliding at 50 nN and after sliding at 100 nN, at velocities ranging from 0.1 to 100 mm s^{-1}, based on Bhushan and Kwak (2007a, 2007b). The solid curve corresponds to the virgin tip profile. At the lower sliding velocity of 0.1 mm s^{-1}, there is an increase in height after the 50 nN wear experiment in the Z-TETRAOL-lubricated samples. This is due to the pick-up of lubricant. Reduction in height indicates tip blunting resulting from wear and is seen in most cases. Wear of the tip could be caused by various mechanisms (Bhushan 2002). Adhesive wear is likely to happen under gentle sliding conditions. Their result provides evidence of an irregularly worn surface, indicating

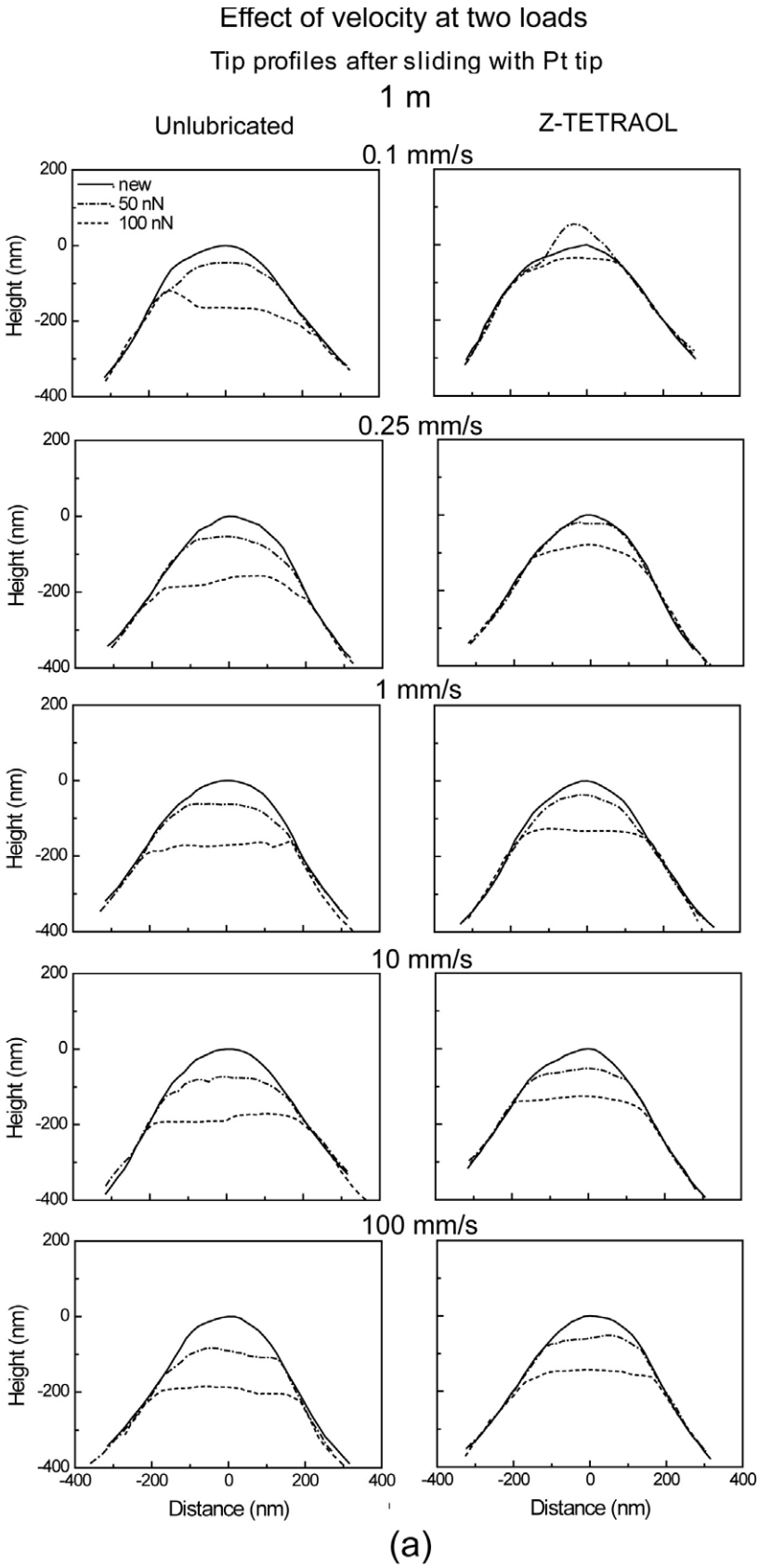

Figure 4. (a) Tip profiles before and after 1 m sliding at 50 nN, after additional 1 m sliding at 100 nN for the sliding velocities at 0.1, 0.25, 1, 10 and 100 mm s^{-1} of the Pt tip on unlubricated and Z-TETRAOL-lubricated samples. (b) Wear volumes and 2D tip radii for Pt tips after 1 m sliding at 50 nN and after additional 1 m sliding at 100 nN as a function of sliding velocity at 0.1, 0.25, 1, 10 and 100 mm s^{-1} on unlubricated and Z-TETRAOL-lubricated samples (Bhushan and Kwak 2007a, 2007b).

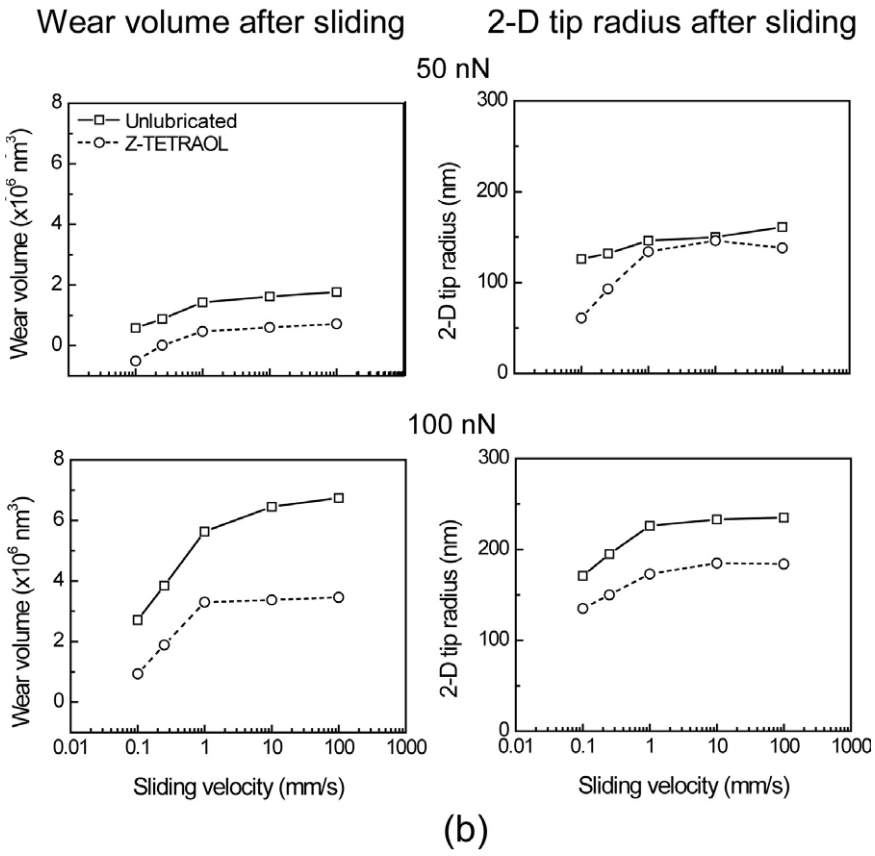

Figure 4. (Continued.)

abrasive wear, especially under high normal load. Brittle Pt-coated silicon asperities can fracture when sliding against the film surface. Particles would be produced by the fracture of asperities. These particles stay between the contacting surfaces and could accelerate the abrasive wear (Tao and Bhushan 2006a, Bhushan and Kwak 2007a).

Wear volumes and tip radii as a function of sliding velocity are plotted in figure 4(b) (Bhushan and Kwak 2007a, 2007b). The wear volume was calculated by comparing the tip profiles before and after sliding. At the sliding velocity of 0.1 mm s^{-1} and the load of 50 nN, the observed increase in height for the lubricated samples corresponds to the negative wear volume and sharper tip radius relative to a new tip, which could be due to the tip picking up lubricant. Initially, wear volume increases rapidly with an increase in the sliding velocity, then it increases slowly but steadily at higher sliding velocities. The Z-TETRAOL-lubricated samples have comparable wear volumes. These ranged from 0.47×10^6 nm^3 to 0.84×10^6 nm^3 after 1 m sliding at 50 nN and from 3.0×10^6 nm^3 to 3.9×10^6 nm^3 after sliding at 100 nN. These are lower than the wear volumes of the unlubricated sample, which ranged from 1.3×10^6 nm^3 to 1.8×10^6 nm^3 at 50 nN and from 5.6×10^6 nm^3 to 6.7×10^6 nm^3 at 100 nN. The data presented in the curves clearly shows that the use of Z-TETRAOL decreases tip wear. The wear volume increases with an increase of velocity. This is typical of adhesive and abrasive wear modes (Bhushan 2002). An increase in wear rate with velocity indicates some tribochemical reaction at the interface, similar to that observed by Tambe and Bhushan (2005a). The wear volume increases as the logarithm of velocity up to between 0.1 and 1 mm s^{-1} and then levels off. This wear behavior at lower sliding velocities is associated with thermally activated atomic-scale stick–slip (Tambe and Bhushan 2005a, Tao and Bhushan 2006c, 2007, Bhushan and Kwak 2007b).

In order to investigate the friction properties between the probe tips and the unlubricated and lubricated film surfaces, the friction force as a function of normal load was measured. On the unlubricated surface, the coefficient of friction (μ) increases from 0.046 to 0.134 after 1 m sliding at 50 nN and to 0.214 after sliding at 100 nN, as shown in figure 5 (Bhushan and Kwak 2007a, Kwak and Bhushan 2008). The increase in the wear volume and tip radius after sliding leads to greater adhesion, which increases the friction force and the measured value of μ. As a reference, the value of μ for an Si substrate is measured as 0.024. The Z-TETRAOL-lubricated samples show lower μ values compared to the unlubricated surface. For the Z-TETRAOL-lubricated sample, μ increased from 0.022 to 0.057 after sliding at 50 nN. It increased further to 0.108 after sliding at 100 nN.

In addition to characterizing the probe tip, the tip shapes after sliding were examined by a scanning electron microscope (SEM). Figure 6 shows SEM images of new probe tips and those obtained after 1 m sliding at 50 nN and after additional 1 m sliding at 100 nN and at sliding velocities of 0.1 mm s^{-1} and 100 mm s^{-1} on unlubricated and lubricated surfaces (Bhushan and Kwak 2007a). Significant wear is observed in

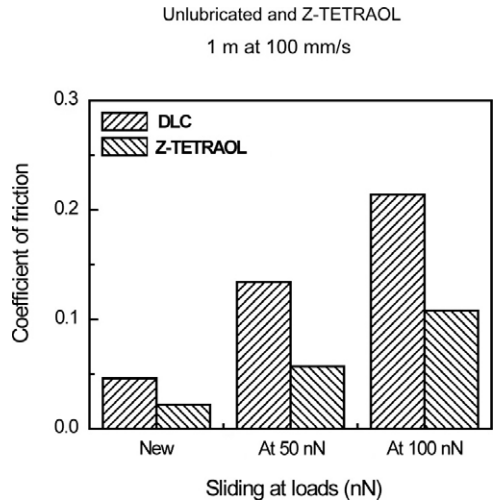

Figure 5. The coefficients of friction after 1 m sliding at 50 nN and after additional 1 m sliding at 100 nN at 100 mm s^{-1} for Pt tip on unlubricated DLC and Z-TETRAOL-lubricated DLC surfaces are presented in the bar chart (Bhushan and Kwak 2007a, Kwak and Bhushan 2008).

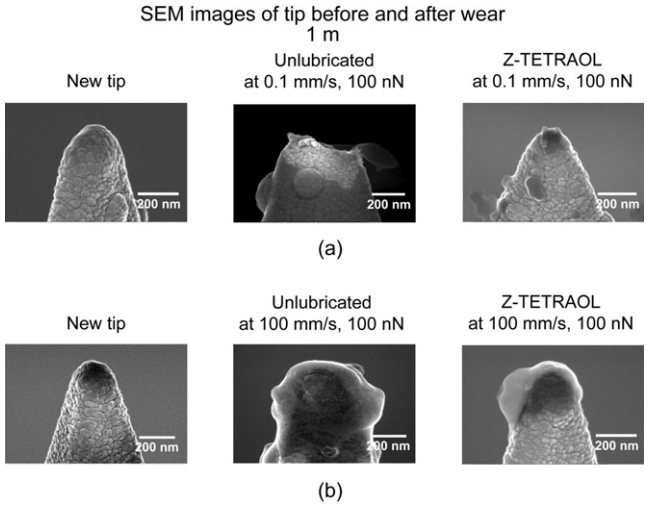

Figure 6. (a) SEM images of an unused Pt tip and Pt tips obtained after 1 m sliding at 50 nN and after additional 1 m sliding at 100 nN and 0.1 mm s^{-1} on unlubricated and Z-TETRAOL-lubricated surface, (b) after 1 m sliding at 100 nN and 100 mm s^{-1} (Bhushan and Kwak 2007a).

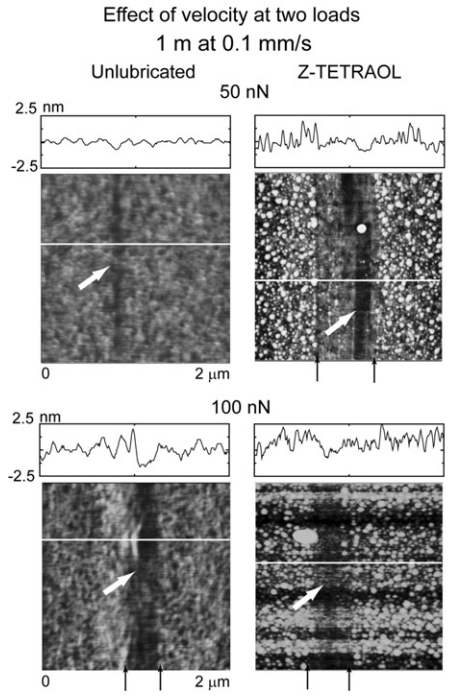

Figure 7. AFM images obtained after 1 m sliding at 50 nN, and after additional 1 m sliding at 100 nN and 100 mm s^{-1} for Pt tip, on unlubricated DLC and Z-TETRAOL film surfaces (Bhushan and Kwak 2007a).

the case of the unlubricated sample surface as compared to the lubricated samples. A lot of debris is observed for tips slid at 100 mm s^{-1}. The Pt-coated tip surface is significantly softer than the DLC sample surface. Average hardness (H) and elastic modulus (E) values at room temperature for bulk Pt and sputtered DLC are 0.42 GPa and 171 GPa (Davis 1998) and 15 GPa and 141 GPa (Bhushan 1999a), respectively. The Pt surface is plastically deformed, implying adhesive wear. Brittle Pt-coated silicon asperities can fracture and generate wear particles which remain trapped, leading to high abrasive wear (Tao and Bhushan 2006a).

Figure 7 shows the height images obtained after 1 m sliding at 50 nN and additional 1 m sliding at 100 nN on unlubricated and Z-TETRAOL-lubricated surfaces at a velocity of 100 mm s^{-1} (Bhushan and Kwak 2007a). On the unlubricated and the Z-TETRAOL-lubricated samples, band-type wear scars result from thermal drift of the z-piezo after line sliding for 167 min obtained after sliding on the same surfaces and at the same loads, but at a velocity of 100 mm s^{-1}. Line profiles are also presented in order to provide more detail. For the unlubricated film surface, the wear regions indicated by the white arrow have depths of about 0.7 and 1.9 nm after sliding at 50 and 100 nN, respectively. The wear scar on the Z-TETRAOL sample is slightly deeper at 50 nN (0.95 nm) but shallower at 100 nN (1.1 nm). The evidence of wear of the DLC surface as well as an increase in wear rate at high velocity suggests that wear mechanisms, in addition to adhesive and abrasive wear, include tribochemical reaction at the interface. The latter involves the phase transformation from a diamond phase to a graphite phase (sp^3 to sp^2) during sliding (Tambe and Bhushan 2005a, 2005b). DLC is an amorphous carbon with a significant fraction of C–C sp^3 bonds along with sp^2 bonds (Bhushan 1999a, 1999b). The tribochemical reaction leads to the formation of a low shear strength surface at the sliding interface, which is easier to remove and is observable as the wear scar. Figure 8 shows a nanowear map generated for a DLC sample by simultaneously varying the normal load and the sliding velocity over the entire scan area (Tambe and Bhushan 2005a). The region of higher wear is observed at the highest normal load and highest sliding velocity, which is consistent with our experimental results.

Temperature plays a crucial role in wear so sliding experiments at 80 °C were conducted at a velocity of

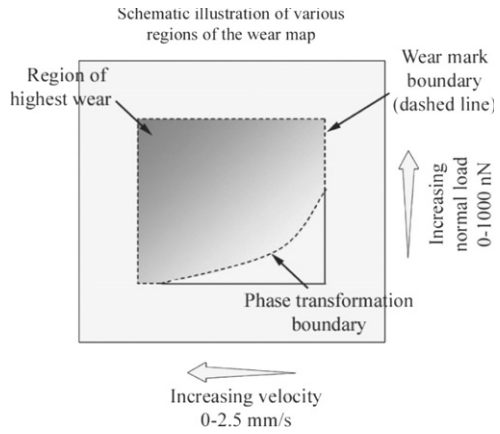

Figure 8. Nanowear map (schematic) illustrating the influence of sliding velocity and normal load on the wear of DLC resulting from phase transformation. The curved area shows debris lining and is indicative of the minimum friction (Tambe and Bhushan 2005a).

0.1 mm s^{-1} (Liu and Bhushan 2003). The wear volume and tip radius data at two loads are plotted in figure 9 (Bhushan and Kwak 2007a, 2008a). At a load of 50 nN, the wear volume is higher at 80 °C than at 20 °C after sliding on the unlubricated sample. Lubricant pick-up is again observed at 80 °C on the Z-TETRAOL-lubricated samples, leading to negative wear volume and a lower tip radius value. However, at 100 nN, the wear volume is positive and increases at a higher test temperature for all three samples. The increased wear volume at higher temperature implies that the tribochemical reaction at the interface is an additional wear mechanism, as suggested earlier.

3.3. Summary

Studies on the phase change chalcogenide medium coated with DLC film and with a Z-TETRAOL lubricant overcoat are reviewed. Pt-coated tips were slid over the films at a range of velocities and loads. Wear has been found to occur by adhesive, abrasive and tribochemical mechanisms. The increase in wear with the logarithm of velocity at lower sliding velocities is associated with thermally activated stick–slip.

The tip sliding on the unlubricated film exhibited a larger volume of wear at a given operating condition and a larger increase of wear volume with an increase in sliding velocity than the tips on Z-TETRAOL-lubricated film surfaces. The tips on the lubricated film surfaces showed minor change of wear volume between 10 and 100 mm s^{-1} of sliding velocity as compared to that between 0.1 and 1 mm s^{-1}, indicating a leveling effect. Based on the results of this study, the lubricated films showed better wear resistance than unlubricated films in the high sliding velocities regime. Temperature was found to have a crucial role in wear. From high temperature experiments, the wear rate at 80 °C is high compared to that at ambient.

4. Nanotribological and nanomechanical characterization—ferroelectric recording technology

Investigations of friction and wear of the Pt-coated tip sliding against PZT film have been performed at a range of loads, velocities and distance by Kwak and Bhushan (2008). Another investigation of friction and wear of various noble-metal-coated tips sliding against a PZT film has been performed for a selected range of loads and sliding distance by Bhushan and Kwak (2008b). In order to relate nanowear to nanomechanical properties, the mechanical properties and the scratch resistance (from nanoindentation) of the PZT substrate and the noble metal coatings used in the probes are reviewed (Palacio and Bhushan 2008a).

The use of Z-TETRAOL and BMIM-PF_6 lubricated on PZT films has been shown to reduce the adhesion, friction and wear of a probe tip. Their properties are summarized in table 3 (Bhushan *et al* 2008b, Palacio and Bhushan 2008a). The two liquids have comparable decomposition temperatures, but the ionic liquid has higher specific heat capacity and thermal conductivity, as shown in the table. Both liquids have very low vapor pressure, which makes them ideal lubricants. Bhushan and Kwak (2008c) investigated the role of lubrication on the sliding of a Pt–Ir-coated tip against PZT films as a function of sliding distance, velocity, temperature and relative humidity, where they elucidated the tip wear mechanisms. An AFM-based method using the surface potential and contact resistance

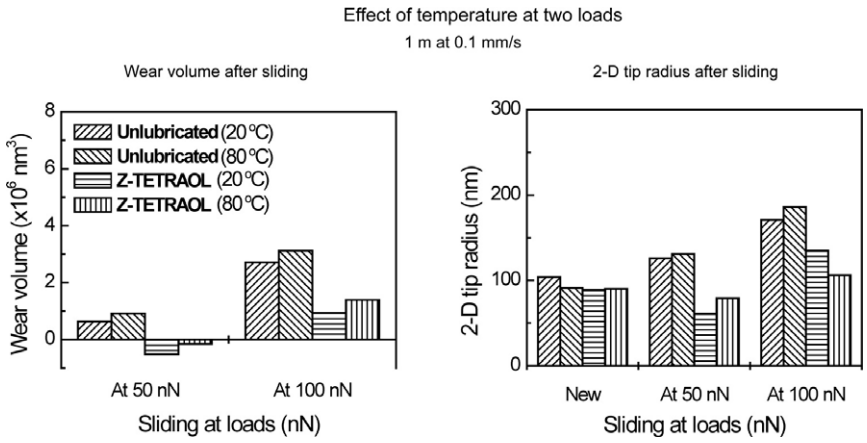

Figure 9. Wear volumes and 2D tip radii as a function of loads after 1 m sliding at 50 nN and after additional 1 m sliding at 100 nN for Pt tip on unlubricated and lubricated DLC film surfaces obtained at sample temperatures of 20 and 80 °C (Bhushan and Kwak 2008a).

to detect wear (Bhushan *et al* 2008b, Palacio and Bhushan 2008c) was used to study unlubricated and lubricated PZT surfaces.

In order to improve the wear resistance of the tips, its mechanical properties need to be optimized while retaining electrical properties. Bhushan *et al* (2008a) reported how a commercial Pt-coated silicon AFM probe was subjected to thermal treatment in order to induce platinum silicide formation at the near-surface. Friction and wear studies of the thermally treated Pt-coated tip sliding against a PZT film were performed at a range of velocities and distances. The mechanical properties and the scratch resistance of the untreated and thermally treated probes have been measured. Using the four-point probe, the electrical resistivity of the films was evaluated and compared to values reported in the literature. Auger electron spectroscopy was used in order to determine the elemental composition in the surface and near-surface and to correlate this to the observed wear behavior of the AFM tip.

Results from these studies will be reviewed here.

4.1. Experimental samples

In the study examining the effect of various experimental parameters on wear, a Pt-coated probe with a Cr underlayer was used, similar to that described in section 3.1 (Bhushan and Kwak 2008b). To compare Pt data with other noble metal coatings, rectangular etched single-crystal silicon cantilevers with pyramidal probe tips coated with Au–Ni, Pt–Ir and Pt–Ni films were selected. (These coated silicon probes will be subsequently referred to in the text individually by the noble metal used.) Details on the probes used in this study are summarized in table 1 (Bhushan and Kwak 2008b). Physical properties of materials used in probes are summarized in table 2 (Palacio and Bhushan 2008b).

In the silicide formation study, Bhushan *et al* (2008a) used a Pt probe without a Cr underlayer. This was a rectangular silicon cantilever coated with 30 nm thick Pt film (NSG01/Pt, NT-MDT, Moscow, Russia). The length and width is 130 μm and 35 μm, respectively. The thermal treatment was undertaken by heating the Pt-coated probe in an N_2 atmosphere at 500 °C for 30 min on a tube furnace (Thermal Products Solutions, New Columbia, PA) (Yin *et al* 2005). The thermally treated probe will be referred to as 'Pt–Si', while the Pt probe that did not undergo this treatment is referred to in the discussion as 'untreated'.

For the PZT disk sample, PZT film was deposited on a 50 nm thick $SrRuO_3$ (SRO) film grown by pulsed laser deposition (PLD) on 0.5 mm thick *c*-axis $SrTiO_3$ (STO) substrate. PLD was also used to grow the 15 nm thick PZT film with a Zr/Ti composition ratio of 20/80 ($PbZr_{0.2}Ti_{0.8}O_3$). The RMS roughness of the PZT film (from a 10 × 10 μm^2 AFM scan) was about 2 nm (Bhushan and Kwak 2008b).

The lubricants used in the Pt probe study were the ionic liquid 1-butyl-3-methylimidazolium hexafluorophosphate, abbreviated as BMIM-PF_6 (Merck), and the perfluoropolyether (PFPE) lubricant Z-TETRAOL (Solvay Solexis Inc.). The two liquids were applied on PZT using the dip coating technique. The method and the apparatus used have been described by Palacio and Bhushan (2008a). Briefly, the test samples were cleaned by ultrasonicating in acetone followed by isopropanol and deionized water for 5 min each. Then, the test sample was vertically submerged into a beaker containing a dilute solution of the lubricant for 10 min. The solutions of the various lubricants are 0.1% (v/v) BMIM-PF_6 in isopropanol and 0.025% (v/v) Z-TETRAOL in HFE 7100 (a solvent consisting of isomers of methoxynonafluorobutane ($C_4F_9OCH_3$)). Both solutions were mixed vigorously and allowed to stand for at least an hour prior to use. The dip coating procedure is as follows. The wafers were pulled up from solution with the aid of the motorized stage set at a constant speed of 5 mm s^{-1} to obtain films of the desired thickness. Thermally treated samples were prepared by heating at 150 °C for 1 h after dip coating. The samples were then measured with an ellipsometer in the fixed refractive index option (NFXD option, Gaertner Scientific L115C Ellipsometer Instruction Manual). The coating thickness was found to be about 3 and 2 nm for BMIM-PF_6 and Z-TETRAOL, respectively. The contact angle of water on the unlubricated and lubricated samples was determined from high magnification surface images.

4.2. Pt-coated tips

Figure 10(a) shows the tip profiles after 1 m sliding at 50 nN and after sliding at 100 nN, at velocities ranging from 0.1 to 100 mm s^{-1} (Kwak and Bhushan 2008). The solid curves correspond to the virgin tip profile. Reduction in height indicates tip blunting resulting from wear and is seen in all cases. The data for wear volumes and tip radii are summarized in figure 10(b) (Kwak and Bhushan 2008). The wear volume was calculated by comparing the tip profiles before and after sliding. Wear of the tip could be caused by various mechanisms, such as adhesive and abrasive wear modes, similar to those discussed in section 3.2 (Bhushan 2002, 2008, Tao and Bhushan 2006a). The initial logarithm dependence is based on the adhesive wear assisted with a thermally activated stick–slip mechanism, similar to that discussed in section 3.2 (Bhushan and Kwak 2007a, 2007b). At higher velocities, impact of asperities becomes important and wear could be caused by the adhesive wear and periodic high velocity impact on the PZT film surface (Tambe and Bhushan 2005a, Tao and Bhushan 2006c, 2007, Kwak and Bhushan 2008).

In order to investigate the friction properties between the probe tips and the PZT film, the friction force as a function of normal load was measured. The data for coefficients of friction are summarized in figure 11 (Kwak and Bhushan 2008). At a sliding velocity of 0.1 mm s^{-1}, the coefficient of friction (μ) increases from 0.020 to 0.029 after 1 m sliding at 50 nN to 0.042 after 1 m sliding at 100 nN. The increase in the wear volume and tip radius after sliding leads to greater adhesion, which increases the friction force and the measured value of μ. As a reference, the value of μ for a Si substrate is measured to be 0.024. At the sliding velocity of 1 mm s^{-1}, μ increased from 0.019 to 0.034 after sliding at 50 nN. It increased further to 0.059 after sliding at 100 nN. The higher velocity of 100 mm s^{-1} showed significantly increased μ values, where the μ increased from 0.021 to 0.043 and 0.093 after sliding

Table 2. Physical properties of materials used in probe tips. (Note: sp.—sputtered.)

Material	Crystal structure	Density (g cm^{-3})	Melting point (°C)	Electrical resistivity at 0 °C ($\mu\Omega$ cm)	Coeff. of linear thermal expansion ($\times 10^{-6}$ °C^{-1})	Tensile strength (MPa)	Elongation in 50 mm (%)	Hardness (GPa)	Elastic modulus (GPa)	Poisson's ratio
Noble metals										
Pt	Fcc[a]	21.45[a]	1769[a]	9.85[a]	9.1[a]	207–241 (as-worked)[a] 124–165 (annealed)	1–3 (as-worked)[a] 30–40 (annealed)	0.91 (as-worked)[a] 0.36 (annealed) 0.42 (as-cast)	171[a]	0.39[a]
Au	Fcc[a]	19.32[a]	1064[a]	2.06[a]	14.2[a]	207–221 (as-worked)[a] 124–138 (annealed)	4 (as-worked)[a] 39–45 (annealed)	0.56 (as-worked)[a] 0.26 (annealed) 0.33 (as-cast)	77[a]	0.42[a]
Ir	Fcc[a]	22.65[a]	2447[a]	4.71[a]	6.8[a]	2070–2480 (hot-worked)[a] 1103–1241 (annealed)	15–18 (hot-worked)[a] 20–22 (annealed)	6.4 (as-worked)[a] 2.2 (annealed) 2.2 (as-cast)	517[a]	0.26[a]
Noble metal alloys										
Pt–Ni	Fcc[b]	—	—	—	—	—	—	—	—	—
Au–Ni (sp.)	Fcc[b]	—	—	—	—	—	—	7[c]	130[c]	—
Other materials										
Ni	Fcc[a]	8.90[a]	1445[a]	6.8[a]	13.3[a]	462 (annealed)[e]	47[e]	0.45 (annealed)[e]	204[a]	0.31[e]
Si(100)	Diamond[e]	2.33[d]	1420[d]	—	42[d]	130[e]	—	13[f]	180[f]	0.28[e]

[a] Davis (1998).
[b] Hultgren *et al* (1963).
[c] Baker and Nix (1994).
[d] Bhushan and Gupta (1991).
[e] Callister (2000).
[f] Bhushan and Li (1997).

Table 3. Physical, thermal and electrical properties of BMIM-PF_6 and Z-TETRAOL.

	1-butyl-3-methylimidazolium hexafluorophosphate (BMIM-PF_6)	Z-TETRAOL
Cation	$C_8H_{15}N_2^+$	—
Anion	PF_6^-	—
Molecular weight (g mol^{-1})	284[a]	2300[b]
$T_{melting}$ (°C)	10[c]	
$T_{decomposition}$ (°C)	300[c]	~320[b]
Density (g cm^{-3})	1.37[a]	1.75[b]
Kinematic viscosity (mm^2 s^{-1})	281[a] (20 °C) 78.7[d] (40 °C)	2000[b] (20 °C)
Pour point (°C)	<−50[e]	−67[b]
Specific heat (J g^{-1} K^{-1})	1.44[f] (25 °C)	~0.20[b](50 °C)
Thermal conductivity at 25 °C (W m^{-1} K^{-1})	0.15[g]	~0.09[b]
Dielectric strength at 25 °C (kV mm^{-1})	—	~30[b]
Volume resistivity (Ω cm)	714[h]	$\sim 10^{13}$[b]
Vapor pressure at 20 °C (Torr)	$<10^{-9}$	$\sim 10^{-12}$[b]
Wettability on Si	Moderate[c]	—
Water contact angle	95°[i]	102°[i]
Miscibility with isopropanol	Total[a]	—
Miscibility with water	—	—

[a] Merck Ionic Liquids Database (2004).
[b] Z-TETRAOL Data Sheet (2002).
[c] Kinzig and Sutor (2005).
[d] Reich *et al* (2003).
[e] Wang *et al* (2004).
[f] Kabo *et al* (2004).
[g] Frez *et al* (2006).
[h] Carda-Broch *et al* (2003).
[i] Palacio and Bhushan (2008a); for comparison, the contact angle of PZT is 88°.

at 50 and 100 nN, respectively. Based on figure 11, friction increases with an increase in the logarithm of velocity which is associated with thermally activated atomic-scale stick–slip (Tambe and Bhushan 2005a, Tao and Bhushan 2006c, 2007, Kwak and Bhushan 2008).

Figure 12 shows SEM images of new probe tips and those obtained after 1 m sliding at 100 nN and at 0.1 mm s^{-1}, 1 mm s^{-1} and 100 mm s^{-1} on the PZT film (Kwak and Bhushan 2008). Significant wear is observed in the case of the higher sliding velocity as compared to those of the lower velocities. The tip wear increases at higher sliding velocities.

Figure 13 shows the surface height images obtained after 1 m sliding at 50 nN and 100 nN on the PZT film at a velocity of 0.1 mm s^{-1} (Kwak and Bhushan 2008). At this velocity, wear scars are observed on the PZT film. However, on both 50 and 100 nN, band-type wear scars result from thermal drift of the z-piezo after sliding along a line for 167 min. If wear scar can be detected, black arrows are used to identify them and white arrows indicate significant damage. The wear depth of about 1 nm is observed after sliding at 50 nN. The line profile shows wear depth in the range of 1.5–2.2 nm after sliding at 100 nN. However, at a velocity of 100 mm s^{-1}, wear scars are not observed on the PZT film. At 100 mm s^{-1}, the sliding cycles are calculated to be 500 cycles lower than those at lower velocities. Although wear scar on the PZT film exists, it cannot be clear due to this small number of sliding cycles.

Temperature plays a crucial role in wear so high temperature experiments were conducted with the sample heated to 80 °C. The temperature of the tip is not the same as the temperature on the sample, but is expected to be lower. At a point contact between tip and sample (nanoscale contact), the dominant heat transfer mechanism is solid–solid conduction which increases linearly with the contact force and saturates above a certain load (Shi and Majumdar 2002). The wear volume and tip radius data at two loads are plotted in figure 14 (Kwak and Bhushan 2008). At a load of 50 nN, the wear volume is higher at a sample temperature of 80 °C than that of 20 °C after sliding on the PZT film.

4.3. Other noble-metal-coated tips

4.3.1. Nanotribological characterization. Wear experiments on the Au–Ni, Pt–Ir and Pt–Ni were conducted to determine how these alloyed coatings perform relative to Pt. In order to determine the maximum normal load which can be used for the wear experiments with the SPIP technique. First the baseline experiments were performed using a Pt tip at loads of 50 nN and 100 nN. The wear experiments were run at 50 nN for 1 m sliding distance, followed by tests at a load of 100 nN for 1 m sliding distance at 10 mm s^{-1} (Bhushan and Kwak 2008b). Figure 15(a) shows Pt tip profiles before and after 1 m of sliding at 10 mm s^{-1} and 50 nN, and after an additional 1 m of sliding at 10 mm s^{-1} and 100 nN on a PZT film (Bhushan and Kwak 2008b). Reduction in height indicates tip blunting resulting from wear and is seen in all cases. Figure 15(b) shows Pt tip profiles taken after sliding for 1, 10, 100 and 300 m for a Pt-coated tip at 100 nN (Bhushan and Kwak 2008b). The data for wear volumes and tip radii are summarized in figure 15(c) (Bhushan and Kwak 2008b). The wear volume and 2D tip radius were obtained as about 9.3×10^6 nm^3 and 223 nm after 100 m sliding, respectively.

Based on the baseline experiments, it was found that a normal load of 100 nN can be used with measurable wear and was selected. Subsequent tests were conducted at a 100 nN load for a sliding distance of the first 100 m at 10 mm s^{-1} and for the remaining 200 m at 100 mm s^{-1}. The wear volume and 2D tip radius as a function of sliding distance are summarized in figure 16 for all tips (Bhushan and Kwak 2008b). The wear volume and 2D tip radius for Au–Ni tips were calculated to be about 3.1×10^6 nm^3 and 176 nm after 100 m sliding at 100 nN, respectively. For Pt–Ir tips, wear volume and 2D tip radius were calculated to be about 3.4×10^6 nm^3 and 115 nm after 100 m sliding at 100 nN, respectively. Data for wear volume and 2D tip radius, shown in figure 16, closely track each other. For Pt–Ni tips, wear volume and 2D tip radius were calculated to be about 7.2×10^6 nm^3 and 257 nm after 100 m sliding at 100 nN, respectively.

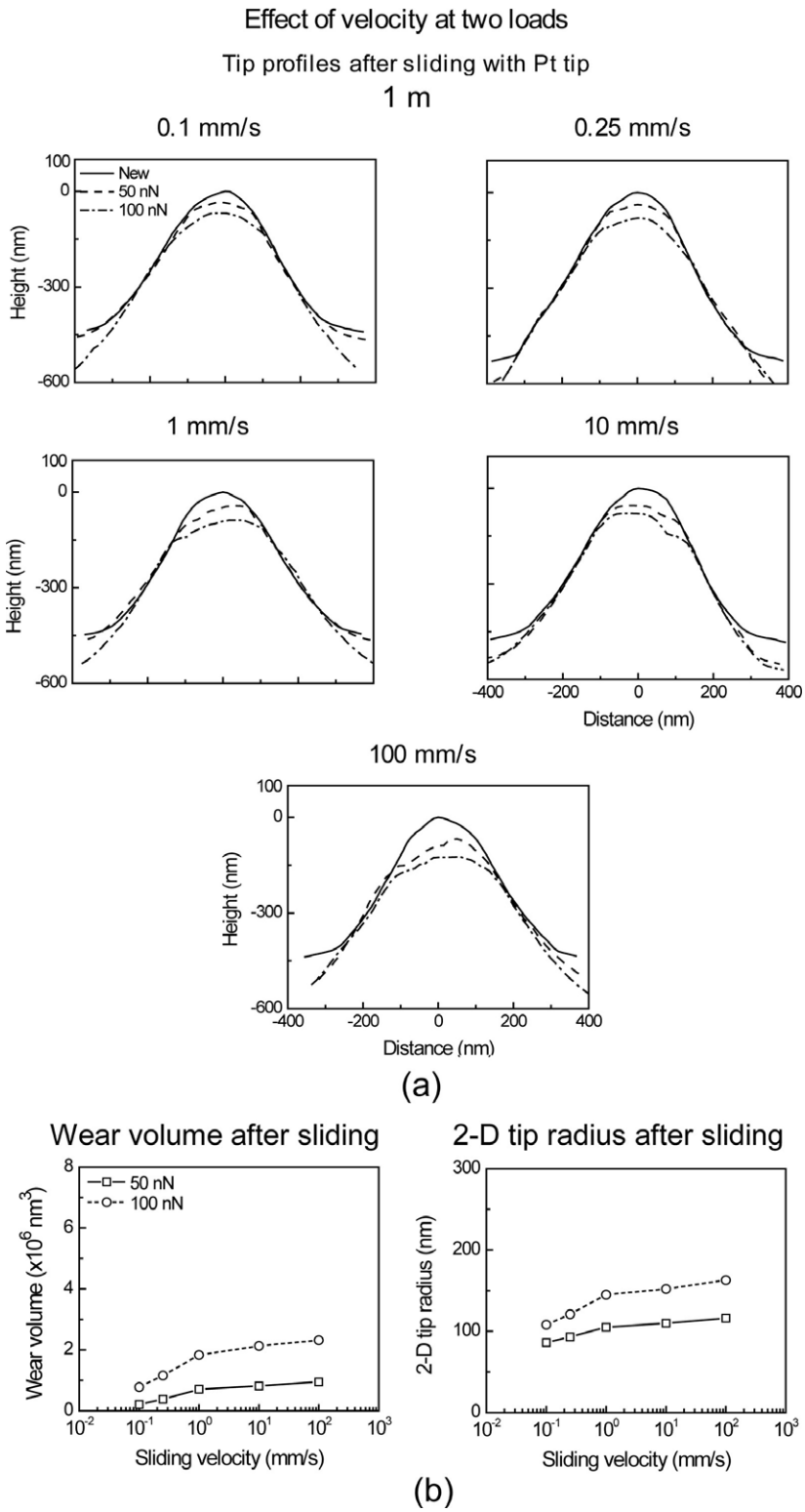

Figure 10. (a) Tip profiles before and after 1 m sliding at 50 nN, after additional 1 m sliding at 100 nN for the sliding velocities at 0.1, 0.25, 1, 10 and 100 mm s^{-1} for Pt tip on the PZT film, and (b) wear volumes and 2D tip radii at 50 and 100 nN as a function of sliding velocity at 0.1, 0.25, 1, 10 and 100 mm s^{-1} for Pt tip on the PZT film (Kwak and Bhushan 2008).

In addition to characterizing the probe tip, the tip shapes after sliding were examined by SEM. Figure 17 shows SEM images of virgin Pt, Au–Ni, Pt–Ir and Pt–Ni tips compared to worn tips after 300 m, 300 m, 300 m and 100 m sliding on the PZT film, respectively (Bhushan and Kwak 2008b). The Pt tip is relatively blunt because the Pt coating is 2–3 times thicker than the other noble metal coatings (table 1). Significant wear is observed in all cases after sliding. The wear of the Pt-coated tip is higher than other metal-coated tips, as noted earlier. The Pt–Ir tip is shown to exhibit less wear compared to the

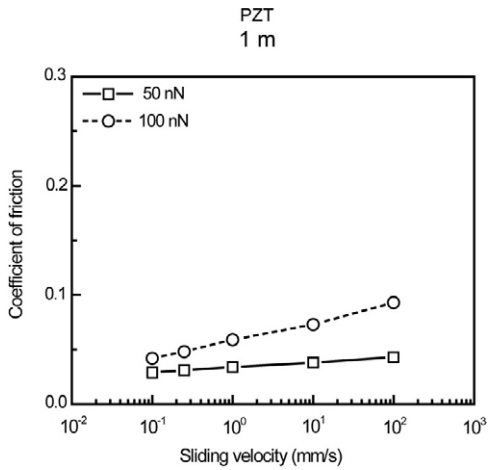

Figure 11. Coefficient of friction after 1 m sliding at 50 nN and after additional 1 m sliding at 100 nN for Pt tip on the PZT film as a function of sliding velocity (Kwak and Bhushan 2008).

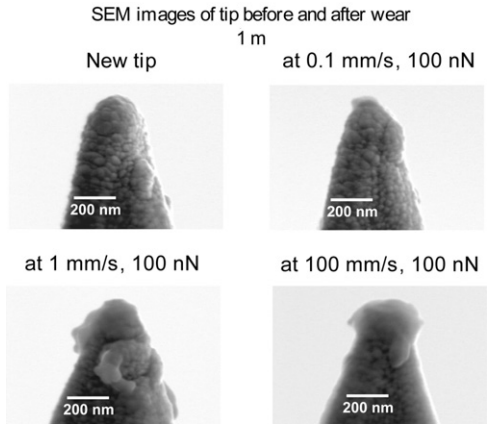

Figure 12. SEM images of a virgin Pt tip and Pt tips obtained after 1 m sliding at 100 nN for the sliding velocities at 0.1, 1 and 100 mm s^{-1} on the PZT film (Kwak and Bhushan 2008).

Au–Ni tip. In particular, the exposed underlayer of the Si part is clearly shown in the Au–Ni tip after 300 m of sliding.

The Pt-coated tip experienced considerable wear as shown in the tip profiles. The Pt-coated tip surface is significantly softer than the PZT film surface (data to be presented in the next section). Alloying of Pt can improve the mechanical properties. Pt–Ni-and Pt–Ir-coated tips are known to have slightly higher hardness and elastic modulus than the Pt tip (data to be presented in the next section). The wear mechanism depends on the tip radius, the tip and sample materials, and operating conditions. Wear of the tip could be caused by various mechanisms (Bhushan 2002, 2008). AFM images of wear scars (not shown here) and SEM images of worn tips show plowing of the PZT material and pile-up in the wear tracks, and plastic deformation of the tip, which is indicative of adhesive wear. Tip profiles provide evidence of an irregularly worn surface, indicating abrasive wear, especially after long sliding distances. Brittle Pt-coated silicon asperities can fracture when sliding against the film surface. Particles would be produced by the fracture of asperities. These particles

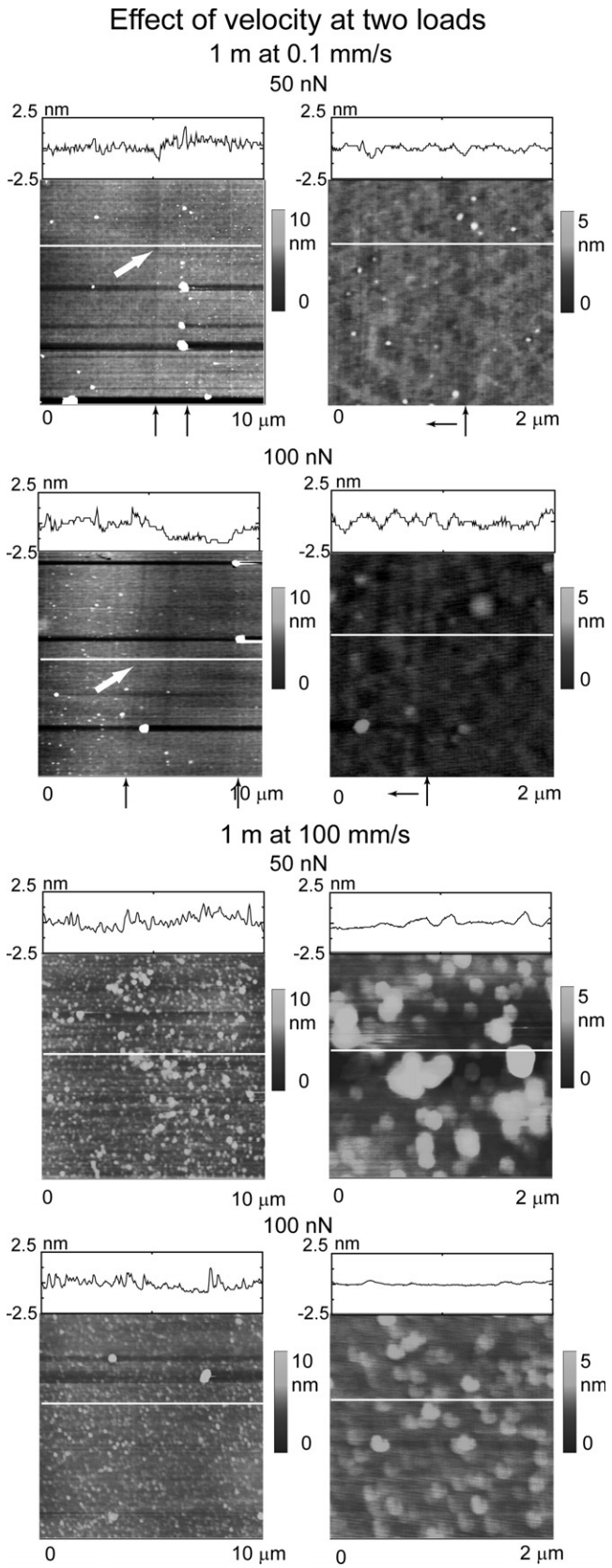

Figure 13. AFM images of wear region on PZT film with scan sizes of 10 × 10 μm^2 and expanded images of 2 × 2 μm^2 obtained after 1 m sliding at 50 nN, and after additional 1 m sliding at 100 nN, and at 0.1 mm s^{-1} and 100 mm s^{-1}. If wear scar can be detected, black arrows are used to identify them and white arrows indicate significant damage (Kwak and Bhushan 2008).

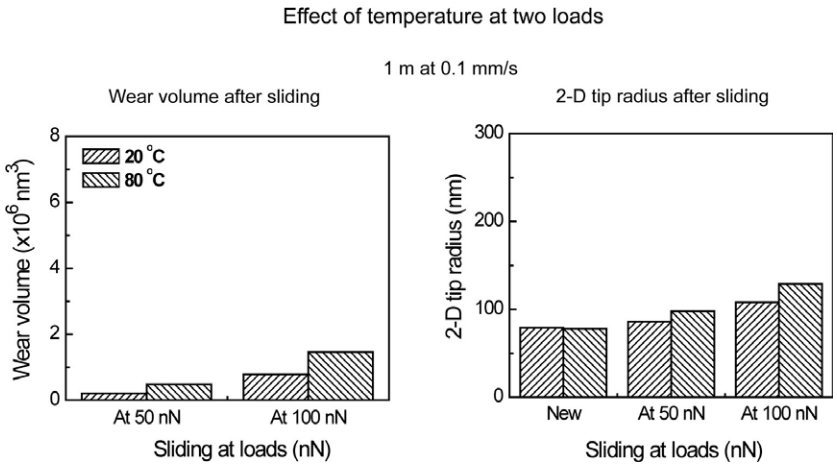

Figure 14. Wear volumes and 2D tip radii as a function of loads after 1 m sliding at 50 nN and after additional 1 m sliding at 100 nN for Pt tips on the PZT film obtained at 20 and 80 °C (Kwak and Bhushan 2008).

stay between the contacting surfaces and could accelerate the abrasive wear (Tao and Bhushan 2006a). At high velocities, the impact of asperities becomes important and wear could be caused by periodic high velocity impact on the PZT film surface (Tambe and Bhushan 2005a, Tao and Bhushan 2007, Bhushan and Kwak 2007a, 2007b, 2008b, Kwak and Bhushan 2008).

4.3.2. Nanomechanical characterization. It is necessary to determine the mechanical properties such as the hardness, elastic modulus and scratch behavior to further understand the observed wear behavior. Palacio and Bhushan (2008a) evaluated the hardness (H) and elastic modulus (E) of the PZT film obtained with the indenter in the continuous stiffness mode, as shown in figure 18. Data points below a contact depth of 10 nm were truncated as they may be artificial. This is due to surface roughness as well as tip calibration limitations (Bhushan and Li 2003). For the E calculations, the ν of PZT was taken as 0.25. The average H and E values are about 13 and 200 GPa, respectively. These values are comparable to those obtained on PZT films deposited using other techniques such as RF magnetron sputtering (Fang *et al* 2003) and higher than the $PbZr_{0.2}Ti_{0.8}O_3$ prepared using the sol–gel method (Chung *et al* 2007). The observed H and E do not change much at deeper penetrations because the underlying material is expected to have comparable mechanical properties. The reported H and E of the $SrTiO_3$ substrate are about 10 and 200 GPa, respectively (Verdyan *et al* 2005).

The scratch behavior of the PZT film is presented in figure 19 (Palacio and Bhushan 2008a). The plot on the left side shows the depth profile before, during and after a scratch, along with the coefficient of friction. SEM images were taken at three areas: at the beginning of the scratch (indicated by 'A' on the friction profile), middle of the scratch ('B') and towards the end of the scratch ('C'). In the scratch profile, it is observed that the tip continuously penetrated the film. The lack of sudden bursts in the surface profile indicates that the film has considerable scratch resistance. The initial coefficient of friction obtained from the nanoscratch experiment is about 0.1. From the SEM images, it can be determined that the scratch test resulted in a combination of plastic (i.e. material pile-up in front of the tip) and brittle (debris particles) deformation modes.

Hardness and elastic modulus of the Pt film and Si substrate as a function of contact depth are shown in figure 20 (Palacio and Bhushan 2008b). The Pt, Pt–Ni, Au–Ni and Si were indented up to 250 nm depth while the Pt–Ir probe was indented to only 50 nm since the latter is much thinner. The hardness and elastic modulus of various noble-metal-coated probes are summarized in data to be presented in figure 23(a) (Palacio and Bhushan 2008b). For materials where the H and E exhibited minimal change (Pt–Ni, Pt–Ir and Si), the average was reported, while for Pt and Au–Ni, the values at 50 nm were used as this is a depth where both surface effects and the substrate influence are both at a minimum, ensuring that it is the actual coating property that is being measured. The alloying of Pt (with Ni) has a significant effect on the modulus and hardness.

Many metallic and ceramic materials (even diamond) are known to creep at temperatures well below half their melting points, even at room temperature (Bhushan *et al* 1996, Bhushan 1999a). Figure 21 shows nanoscale creep data for the various metal-coated probes and Si, where the change in displacement, mean stress and contact stiffness was monitored while holding the tip at the maximum imposed load (P_{max}) (Palacio and Bhushan 2008b). A lower P_{max} was applied on Pt–Ir as it is a very thin coating; the selected load of 250 μN ensures that the tip is measuring the creep resistance of the coating and did not penetrate the substrate during the creep experiment. From the displacement plots, it is observed that the three alloyed coatings (Pt–Ni, Pt–Ir and Au–Ni) exhibited less creep compared to Pt. The Si surface also shows significant creep, which is consistent with previous reports. This creep on silicon is a combination of two factors: initial creep can occur as the tip penetrates the native oxide surface, which is then followed by a dislocation glide plasticity mechanism (Bhushan *et al* 1996).

Palacio and Bhushan (2008b) also examined the scratch behavior of the coatings, figure 22. The plot on the

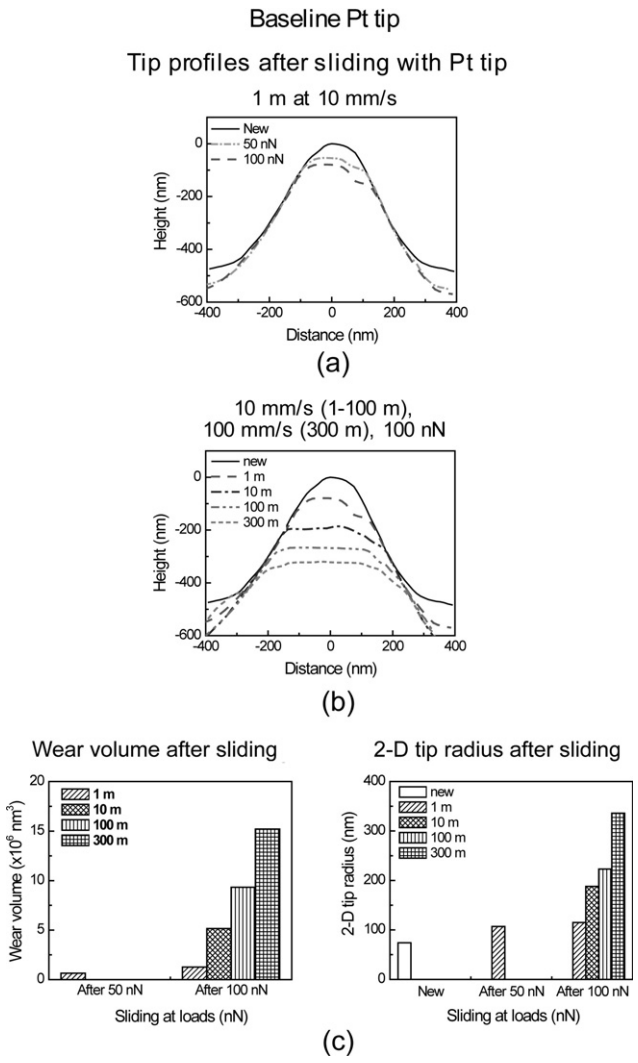

Figure 15. (a) Tip profiles before and after 1 m sliding, 10 mm s^{-1} and at 50 nN, after additional 1 m sliding at 100 nN for Pt tip on a PZT film, (b) tip profiles before and after 1, 10 and 100 m sliding at 10 mm s^{-1}, and 300 m sliding at 100 mm s^{-1} and at 100 nN on the same film. The solid curve corresponds to the virgin tip profile, and (c) wear volumes and 2D tip radii after 1 m at 50 nN and 1, 10 and 100 m sliding at 10 mm s^{-1}, and 300 m sliding at 100 mm s^{-1} (Bhushan and Kwak 2008b).

left-hand side shows the depth profile before, during and after a scratch, along with the coefficient of friction. The critical load to failure of the coating is summarized in figure 23(b). SEM images were taken at three areas: at the beginning of the scratch (indicated by 'A' on the friction profile), middle of the scratch ('B') and towards the end of the scratch ('C'). In the scratch profiles, it is observed that the tip continuously penetrated the coatings. The lack of sudden bursts in the surface profiles indicates that the coatings have considerable scratch resistance. Among the four coatings studied, Pt–Ir exhibited the greatest scratch resistance as evidenced by the low penetration depth observed. From the SEM images, it can be determined that the deformation mode from the scratch experiments is mainly plastic deformation, as seen from material pile-up in front of the tip. The scratch profiles and SEM images (mainly from region B) were used to create a damage index bar chart, shown in figure 23(c) (Li and Bhushan 2001, Palacio and Bhushan 2008b). In this qualitative approach, 0 represents no damage, 1 small damage, 2 medium damage, 3 large damage and 4 severe damage. Both Pt and Au–Ni were determined to have a damage index of 3 because the scratch track of Pt is wide and shallow while that of AuNi is narrow and deep, such that the extent of coating deformation is almost the same. However, from region C, the pile-up in Pt is more severe, so it is concluded that this coating is the least scratch-resistant overall.

These findings can be correlated to wear results shown in figure 23(d), obtained from figure 16 at 10 m at a load of 100 nN (Bhushan and Kwak 2008b, Palacio and Bhushan 2008b). Here it is observed that all alloyed coatings exhibit significantly less wear compared to Pt. The Pt–Ir shows the lowest wear, while Pt–Ni and Au–Ni have comparable wear volumes. This is similar to the results shown in figure 22, where Pt–Ir and Pt have the smallest and greatest damage at region C, respectively (Palacio and Bhushan 2008b).

4.3.3. Role of lubricants, scanning velocity and operating environment. Wear experiments were conducted with the unlubricated and lubricated PZT films at 50 and 100 nN in order to compare the wear resistance of the Pt–Ir tip. Data on wear and tip radius as a function of sliding distance is presented in figure 24 (Bhushan and Kwak 2008c). After sliding for 300 m, the Pt–Ir tip profile against Z-TETRAOL-lubricated film showed less wear compared to that against the unlubricated PZT film. Ionic liquid also provides wear protection but less than that of Z-TETRAOL. Tip profiles (not shown here) provide evidence of an irregular worn surface, indicating abrasive wear, especially after long sliding distances. Brittle Pt–Ir-coated silicon asperities can fracture when sliding against the film surface. Particles would be produced by the fracture of asperities. These particles stay between the contacting surfaces and could accelerate the abrasive wear (Bhushan 2002, 2008, Tao and Bhushan 2006a).

The magnitude of the wear volume and its rate of increase against Z-TETRAOL-lubricated films are lower than that against the unlubricated PZT film. The BMIM-PF_6-lubricated film also provides wear protection but less than that of Z-TETRAOL. The ions in BMIM-PF_6 can attract water molecules, which can permeate through the lubricant film and compete with the lubricant molecules bonded to the PZT. In all cases, the increase in wear volume is more significant at larger sliding distances, and the progressive damage is responsible for an increase in the wear rate. For example, the wear volumes against the unlubricated film and the Z-TETRAOL-lubricated film after sliding for a distance of 100 m are 3.4×10^6 and 2.8×10^6 nm^3. However, after sliding for 300 m they are 6.6×10^6 and 4.2×10^6 nm^3, respectively.

In order to investigate the friction properties between the tips and the PZT films, the coefficient of friction was measured during the test. As shown in figure 24, the coefficient of friction increases with an increase in the sliding distance (Bhushan and Kwak 2008c). The rate of increase is higher at larger sliding distances, consistent with the trends in wear volume. For example, the coefficients of friction against the unlubricated

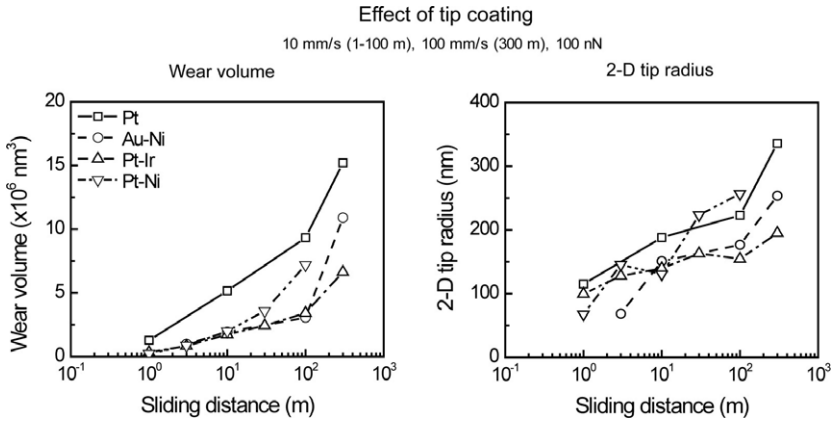

Figure 16. Wear volumes and 2D tip radii plotted as a function of sliding distance for Pt, Au–Ni, Pt–Ir and Pt–Ni tips on the PZT film (Bhushan and Kwak 2008b).

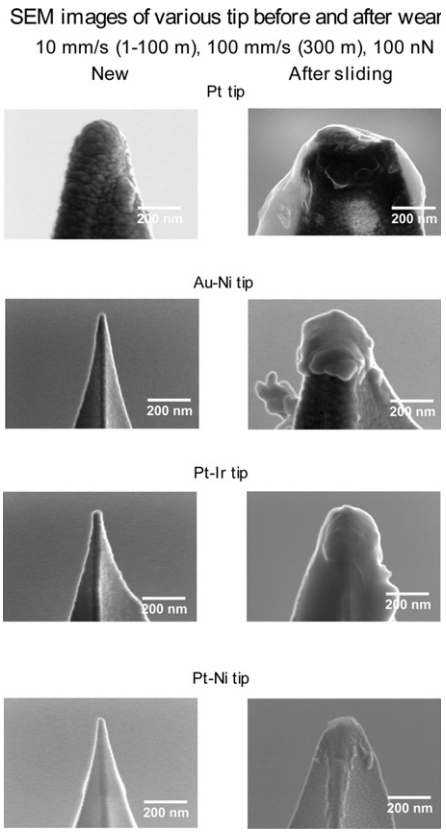

Figure 17. SEM images of the Pt, Au–Ni, Pt–Ir and Pt–Ni tips obtained before and after sliding at 100 nN on the PZT film for 300 m, 300 m, 300 m and 100 m, respectively (Bhushan and Kwak 2008b).

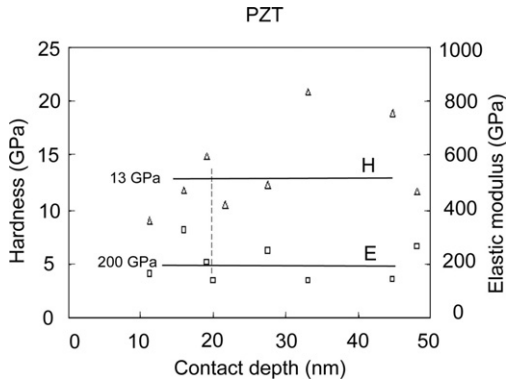

Figure 18. Hardness and elastic modulus of the PZT film. The dashed line indicates that data below 20 nm contact depth may be susceptible to surface roughness and tip imperfection effects (Palacio and Bhushan 2008a).

film and the Z-TETRAOL-lubricated film after sliding for a distance of 100 m are 0.14 and 0.08: however, after sliding for 300 m they are 0.2 and 0.11, respectively.

Figure 24 also summarizes the adhesive force as a function of sliding distance (Bhushan and Kwak 2008c). The value of the adhesive force at a given sliding distance against the Z-TETRAOL-lubricated film is consistently lower than that against the unlubricated PZT film. The BMIM-PF_6 lubricated film presents comparable value but higher than that of Z-TETRAOL. The increase in the tip radius after sliding leads to a larger contact area leading to higher adhesion, which increases the friction force and the measured value of μ. For example, the adhesive force for unlubricated film and the Z-TETRAOL-lubricated film after sliding for a distance for 100 m are 99 and 48 nN, and the tip radius after sliding for 100 m are 155 and 137 nm, respectively. It is noted that the rate of increase is higher at larger sliding distances, which is consistent with the trends in wear volume and coefficient of friction.

Figure 25 shows SEM images of Pt–Ir tips before the wear experiments and after sliding for 300 m at a load of 100 nN (Bhushan and Kwak 2008c). Blunting of the Pt–Ir tip against the Z-TETRAOL-lubricated film occurred to a lesser extent against the unlubricated film. In particular, the exposed underlayer of the Si part is clearly observed in the tip against the unlubricated film. The post-wear experimental images corroborate the 2D tip profiles. The tip is plastically deformed during wear; therefore, it can be deduced that the mechanism for tip wear is adhesive.

From SEM imaging and tip profiling, as well as AFM imaging of the PZT films (not shown here), it was found that

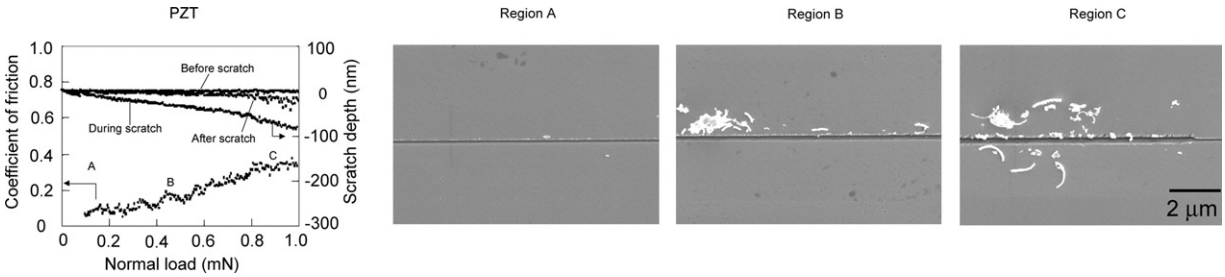

Figure 19. Scratch depth profile and coefficient of friction as a function of increasing normal load for PZT. SEM images were taken at three regions: at the beginning of the scratch ('A'), in the middle of the scratch ('B') and at the end of the scratch ('C') (Palacio and Bhushan 2008a).

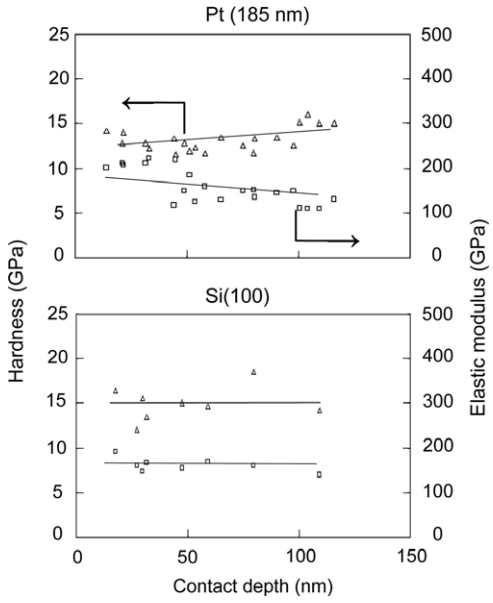

Figure 20. Hardness and elastic modulus of the Pt-coated AFM probe and Si(100) as a function of contact depth greater than 10 nm.

the Pt–Ir tips exhibit adhesive and abrasive wear (Bhushan and Kwak 2008c). The wear, friction and adhesive forces increase with sliding distance, and the rate of increase is higher at larger sliding distances. The Z-TETRAOL-lubricated film exhibited the best performance and was selected for velocity, temperature and relative humidity studies.

In order to study the effect of velocity, wear experiments were conducted using an AFM at a velocity range of 0.1–100 mm s^{-1} and the data are presented in figure 26 (Bhushan and Kwak 2008c). The Z-TETRAOL-lubricated film exhibits lower wear volumes than that of the unlubricated film. In the velocity range used, wear volumes ranged from 0.04×10^6 to 0.41×10^6 nm^3 after sliding at 50 nN and from 0.11×10^6 to 0.92×10^6 nm^3 after sliding at 100 nN. These are lower than the wear volumes of the unlubricated sample, which ranged from 0.07×10^6 to 0.61×10^6 nm^3 after sliding at 50 nN and from 0.19×10^6 to 1.3×10^6 nm^3 after sliding at 100 nN, in the velocity range used. The data presented clearly show that the use of Z-TETRAOL decreases tip wear. The tip radii and corresponding wear volume data for the unlubricated and lubricated films follow a similar trend.

It can be observed in figure 26 that wear volume initially increases as a logarithm of sliding velocity at two loads, and then it increases with sliding velocity at a slower rate with a velocity exponent in the range of 0.06–0.11 (Bhushan and Kwak 2008c). Also, the coefficient of friction initially increases as a logarithm of sliding velocity at two loads, and then it increases with sliding velocity at a slower rate with a velocity exponent in the range of 0.017–0.021. The initial logarithm dependence for both friction and wear is based on the thermally activated stick–slip mechanism (Tambe and Bhushan 2005a, Tao and Bhushan 2006c, 2007, Bhushan and Kwak 2008c). At higher velocities, the impact of asperities becomes important, and wear could be caused by the adhesive wear and periodic high velocity impact on the PZT film surface (Tambe and Bhushan 2005a, Tao and Bhushan 2007, Bhushan and Kwak 2007a, 2007b, 2008c, Kwak and Bhushan 2008).

Temperature plays a crucial role in wear, so high temperature experiments were conducted with the sample heated to 80 and 120 °C (Bhushan and Kwak 2008c). Figure 27 shows the wear volume, tip radius and coefficient of friction data after 1 m sliding at 50 nN, after an additional 1 m sliding at 100 nN and 0.1 mm s^{-1} for sample temperatures at 22, 80 and 120 °C (Bhushan and Kwak 2008c). The temperature of the tip is expected to be lower than the temperature of the sample. Bhushan and Kwak (2008a) have reported the temperature difference to be of the order of 6 °C when the sample is heated to 80 °C. Based on the high temperature data in figure 27, wear rate increases with an increase in the sample temperature (Bhushan and Kwak 2008c). The tip sliding on the unlubricated film exhibited a larger volume of wear at a given operating condition than that on Z-TETRAOL-lubricated film surfaces.

It should be noted that the thickness of the surface water layer is expected to decrease at higher temperature, which is responsible for meniscus forces. However, this source does not appear to be important for changes in friction and wear as a function of temperature at the ambient humidity. For the PZT film, domain walls and microstructure affect the mechanical and electrical properties (Setter *et al* 2006), which govern friction and wear behavior. The domain wall displacement is expected to occur with an increase of temperature, which is believed to be responsible for an increase in friction and wear. The relationship between the domain configuration and the microstructure, friction and wear properties still needs to

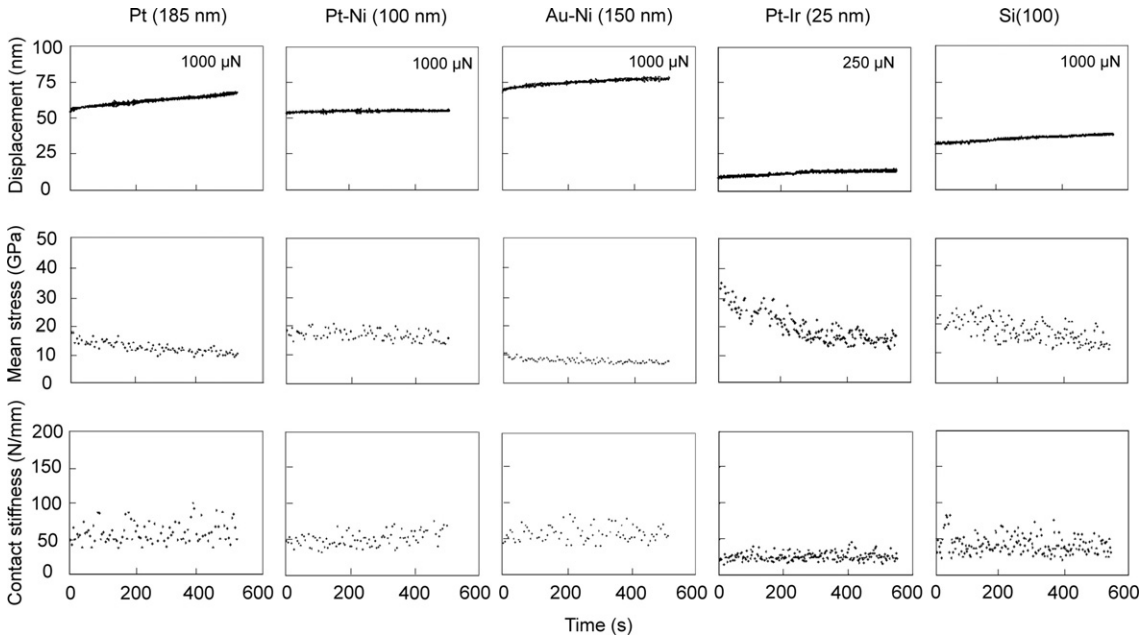

Figure 21. Creep displacement, mean stress and contact stiffness as a function of time of the various metal-coated AFM probes and Si(100) (Palacio and Bhushan 2008b).

be understood. In experiments with PZT lubricated with a thin film of Z-TETRAOL, the effect of the temperature appears to be similar to that of the unlubricated PZT surface; thus, the effect of temperature on the lubricated PZT is dominated by the PZT substrate. The lubricant merely reduces friction and wear at a given temperature.

In order to study the effect of humidity, wear experiments were conducted at 5–80% RH. Figure 28 shows the wear volume, tip radius and coefficient of friction data after 1 m sliding at 50 nN, after additional 1 m sliding at 100 nN and 0.1 mm s^{-1} at 5, 50 and 80% RH (Bhushan and Kwak 2008c). Based on the data, the wear volume, tip radius and coefficient of friction all increase with relative humidity. Using the schematic in figure 29, surface water layer is expected to develop for the unlubricated PZT film, and its thickness should increase with relative humidity (Bhushan and Kwak 2008c). This increase in meniscus thickness is expected to result in an increase of meniscus force, and is responsible for an increase in wear volume and friction (see solid lines in figure 28) (Bhushan and Kwak 2008c). The rate of increase of friction and wear is relatively constant during the entire humidity range.

In the case of the Z-TETRAOL-lubricated film, the friction and wear increase slightly up to 50% RH and increase at a higher rate at higher humidity (see dotted lines in figure 28). Surface water molecules are expected to aggregate with mobile lubricant fractions of Z-TETRAOL and form a large meniscus, which is responsible for an increase in wear volume and coefficient of friction at a higher rate at a high humidity of 80% RH, as illustrated in figure 29 (Bhushan and Kwak 2008c).

To gain more insight into the effect of lubrication on the PZT surface, Palacio and Bhushan (2008a) evaluated the nanoscale adhesive force and coefficient of friction measurements on the lubricated and unlubricated PZT using an Si_3N_4 tip, as shown in figure 30(a). The coefficient of friction of the unlubricated PZT is about 0.04, which is lower than that obtained from nanoscratch (0.1, presented in figure 19). This is attributed to the difference in the length scales and the loads involved in the two techniques.

The lower portion of figure 30(a) is a schematic illustrating the role of meniscus formation in the adhesive and friction forces obtained for the surfaces of interest. On the unlubricated sample, water is likely to form a meniscus as the tip approaches the surface. This is less likely to occur with the lubricated sample, having low surface energy, leading to lower adhesion and friction forces. Both Z-TETRAOL and BMIM-PF_6 were able to reduce the tip–surface adhesive force and coefficient of friction, with the former exhibiting slightly better performance. The higher adhesive force and coefficient of friction observed in BMIM-PF_6 could be due to the ions attracting water molecules and facilitating meniscus formation.

Figure 30(b) presents plots of the coefficient of friction as a function of the number of sliding cycles at 70 nN normal load (Palacio and Bhushan 2008a). Only a small rise in the coefficient of friction was observed for both Z-TETRAOL and the BMIM-PF_6 surfaces, indicating low surface wear. In contrast, the unlubricated PZT is showing a gradual increase, possibly indicating surface wear. This data further illustrates the role of lubrication, as well as the choice of the lubricant preparation method on enhancing surface durability. The thermal treatment procedure facilitates the creation of mobile and immobile lubricant fractions. During the cycling test, repeated sliding of the tip can remove the lubricant that is attached to the substrate. But at the same time, the mobile fraction can flow to the test area and replenish the lubricant on the surface, such that the friction force does not change. A rise in the friction force is indicative of lubricant removal and wear of the substrate surface.

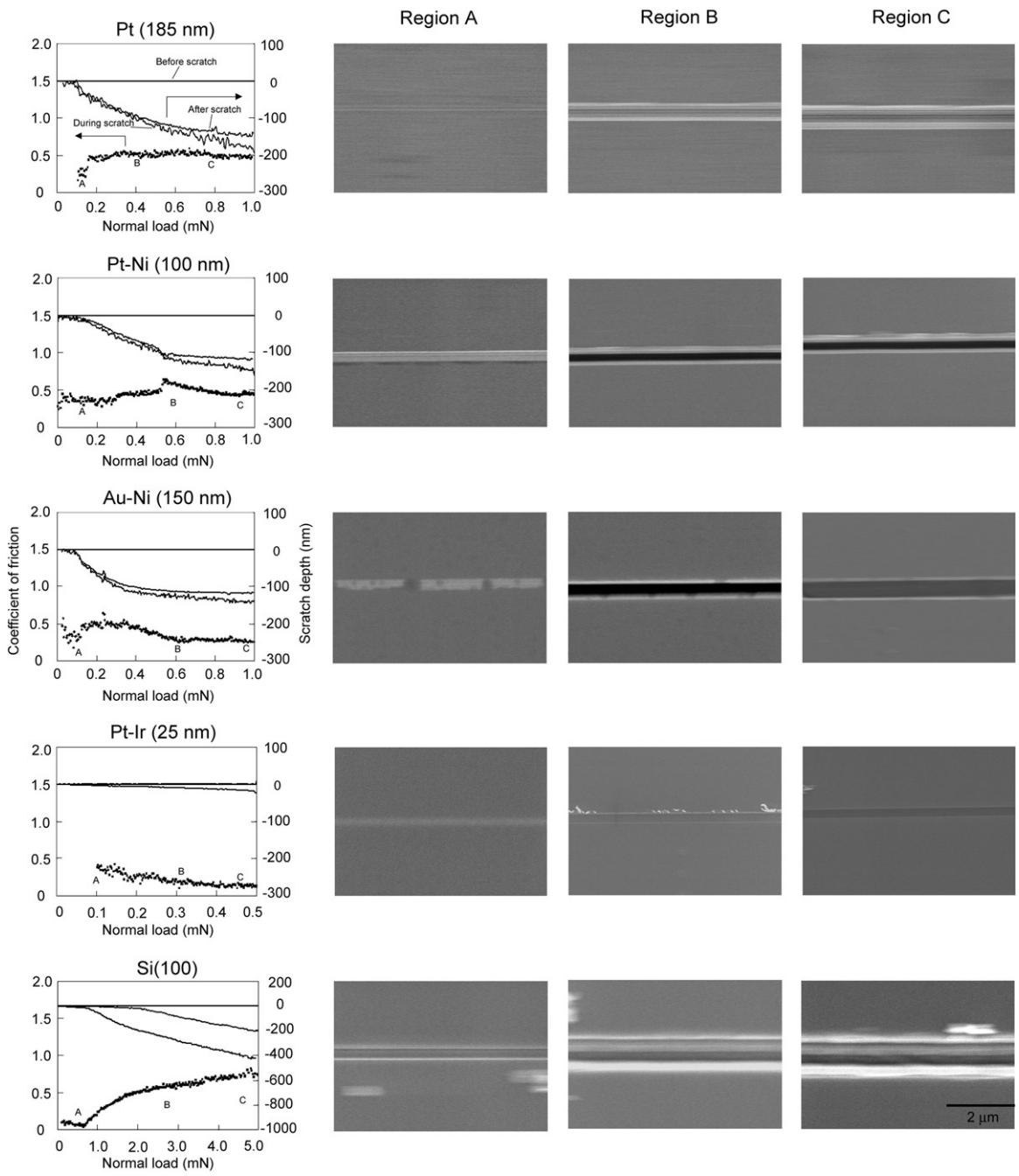

Figure 22. Scratch depth profile and coefficient of friction as a function of increasing normal load for the metal-coated probes and Si(100). SEM images were taken at three regions: at the beginning of the scratch ('A'), in the middle of the scratch ('B') and at the end of the scratch ('C'). A higher load was used on Si in order to generate observable surface damage (Palacio and Bhushan 2008b).

The wear experiments conducted for subsequent surface potential and contact resistance characterization involved the use of a higher load (5 μN) and higher speed (600 μm s^{-1}) compared to those used for the durability study discussed above. The conditions used facilitated the creation of easily identifiable wear scars. Figure 31(a) shows images taken after wear testing on the surface where a diamond tip was used to create wear scars with 5 × 5 μm^2 dimensions (Palacio and Bhushan 2008a). The surface height map is shown in the left column and the surface potential image is on the right. The unlubricated PZT sample has the deepest scar, implying that both Z-TETRAOL and BMIM-PF$_6$ were able to protect the PZT surface from wear. As shown in the bar plot in figure 31(b), the surface potential change is most pronounced on the PZT surface because it experienced the most wear (Palacio and Bhushan 2008a). This comes from charge build-up during the sliding (Palacio and Bhushan 2007, 2008c). Since PZT is nonconducting, these charges do not get dissipated and remain on the surface.

The contact resistance of the surface was also measured and the results are shown in figure 32 (Palacio and Bhushan 2008a). PZT does not show a resistance change indicating

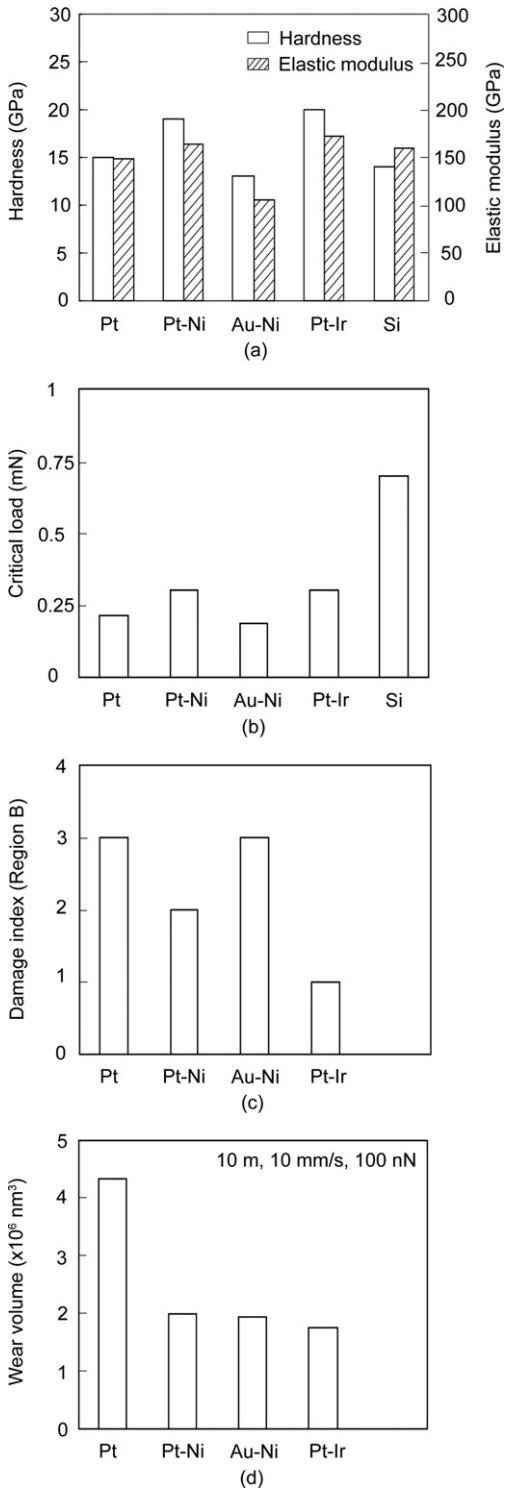

Figure 23. Bar plot summarizing (a) hardness and elastic modulus. (b) Critical load to failure of the surface from scratch testing. (c) Damage index and (d) wear volume of Pt-, Pt–Ni-, Au–Ni- and Pt–Ir-coated AFM tips. Data for Si(100) is provided in (a) and (b) for reference. The reported H and E are based on the average value for Pt–Ir, and taken at 50 nm for Pt, Pt–Ni and Au–Ni. The critical load is obtained from the friction profiles in figure 22 and the damage index chart is based on SEM examination of the scratch track in the middle of the scratch from figure 22 (0 represents no damage, 1 small damage, 2 medium damage, 3 large damage and 4 severe damage). The wear volume is determined at 10 m at a load of 100 nN from figure 16 (Palacio and Bhushan 2008b).

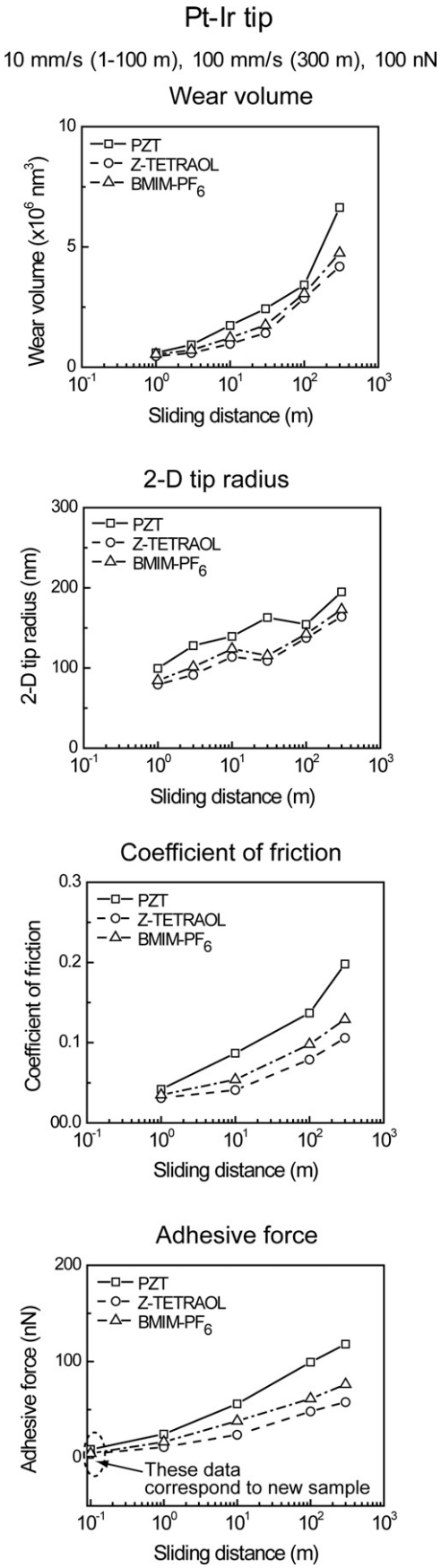

Figure 24. Wear volumes, 2D tip radii, coefficient of friction and adhesive force as a function of sliding distance for Pt–Ir tips on the unlubricated, Z-TETRAOL- and BMIM-PF_6-lubricated PZT films (Bhushan and Kwak 2008c).

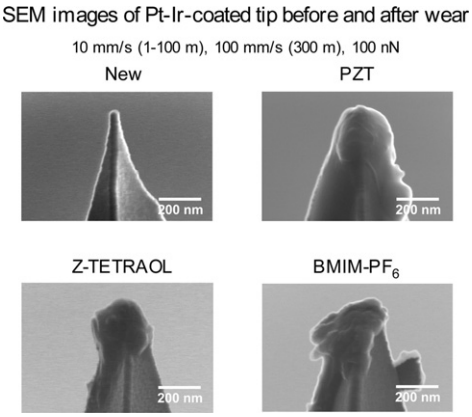

Figure 25. SEM images of Pt–Ir tips obtained before and after 300 m sliding at 100 nN on the unlubricated, Z-TETRAOL- and BMIM-PF_6-lubricated PZT films (Bhushan and Kwak 2008c).

the newly exposed surface is still PZT, i.e. the tip did not go through the entire thickness of the film during the test. Tests on the Z-TETRAOL- and BMIM-PF_6-lubricated surfaces did not show any observable change in the contact resistance, indicating that some lubricant may still be present on the surface and the underlying substrate is not fully exposed. In contrast, wear tests on an Au film on silicon exhibit a large change in the resistance, indicating that the technique can detect coating removal and substrate exposure (Palacio and Bhushan 2007).

One of the concerns in the wear experiments on the lubricated PZT samples is frictional heating. The high temperature that could be generated during sliding may possibly degrade the thin lubricant film. The interface temperature rise between the PZT surface and the diamond tip has been calculated by Palacio and Bhushan (2008a). This case was evaluated due to the high load and high speed used, which was necessary for surface potential and contact resistance measurements (figures 31 and 32). For simplicity, the thermal effect on the lubricant was neglected since this layer is extremely thin and the applied load is borne by the substrate.

In order to carry out the thermal analysis, first, the Peclet number, L is calculated to determine if the sliding falls into the low speed, intermediate or high speed case (Bhushan 2002):

$$L = \frac{3Vd_{\max}}{16\kappa}. \tag{1}$$

Here, V is the sliding speed, $d_{\max}$ is the maximum contact diameter and κ is the thermal diffusivity of the material (PZT). The $d_{\max}$ is calculated from the contact area, A:

$$A = \pi \frac{d_{\max}^2}{4} \tag{2}$$

where A is the ratio of the applied load and the hardness for an interface going through plastic deformation at the high loads used. The contact area A is calculated as 3.8×10^{-16} m^2. The thermal diffusivity is a known value and is given in table 4 (Palacio and Bhushan 2008a). The calculated value for the Peclet number L, 2×10^{-6}, is less than 0.5, so this experimental condition is at the low speed sliding regime.

Table 4. Selected physical and thermal properties of bulk PZT and polycrystalline diamond.

		PZT	Poly. diamond
Physical	Elastic modulus, E (GPa)	200	1140[a]
	Hardness, H (GPa)	13	80[a,b]
	Poisson's ratio, ν	0.25[c]	0.07[a]
	Density (kg m^{-3})	7.8×10^3	
Thermal	Thermal conductivity, k (W m^{-1} K^{-1})	1.60[d] (@ 227 °C)	400[a]
	Thermal diffusivity, κ (m^2 s^{-1})	0.60×10^{-6},[d] (@227 °C)	—
	Specific heat at constant pressure, c_p (kJ kg^{-1} K^{-1})	0.34[d] (@ 227 °C)	0.52[a] (@ 27 °C)

[a]Field (1992).
[b]Bhushan and Gupta (1991).
[c] Assumed.
[d]Morimoto *et al* (2003).

For the low speed sliding case, where the partition of heat between the two bodies is considered, the temperature rise (θ) on the PZT surface is given by (Bhushan 2002)

$$\theta = \frac{0.33\mu H V d_{\max}}{k + k_t}. \tag{3}$$

In equation (3), μ is the coefficient of friction (0.04 from figure 30(a)), H is the hardness of PZT (presented earlier), and k and k_t are the thermal conductivities of PZT and the diamond tip, respectively (both given in table 4). The resulting temperature change on the PZT layer was found to be only 3.2×10^{-6} °C. Based on this analysis, it can be seen that a negligible temperature change is observed due to the very low sliding velocity used in their experiment. This implies that the temperature rise generated from sliding will not affect or degrade the lubricant layer on the PZT.

4.4. Surface-treated tips

4.4.1. Nanotribological characterization. Bhushan *et al* (2008a) subjected the Pt tip (without an underlayer) to thermal treatment with the goal of improving its wear resistance. To compare the wear resistance of the Pt and Pt–Si tips, wear experiments were performed by sliding the tips on PZT films at a load of 100 nN. Figure 33(a) shows tip profiles taken after sliding for 1, 10, 100 and 300 m (Bhushan *et al* 2008a). These profiles were compared with one taken before the wear experiment in order to calculate the wear volume. After sliding for 300 m, the Pt–Si tip profile showed less wear compared to the Pt tip. This is confirmed in figure 33(b), which summarizes the wear volume and the 2D tip radius as a function of sliding distance (Bhushan *et al* 2008a). It must be noted that the wear volume is the preferred method to evaluate tip wear compared to tip height information, because the volume reflects the change in both the height and the width of the base of the worn region. The magnitude of the wear volume and its rate of increase for the Pt tip are consistently higher than Pt–Si. What

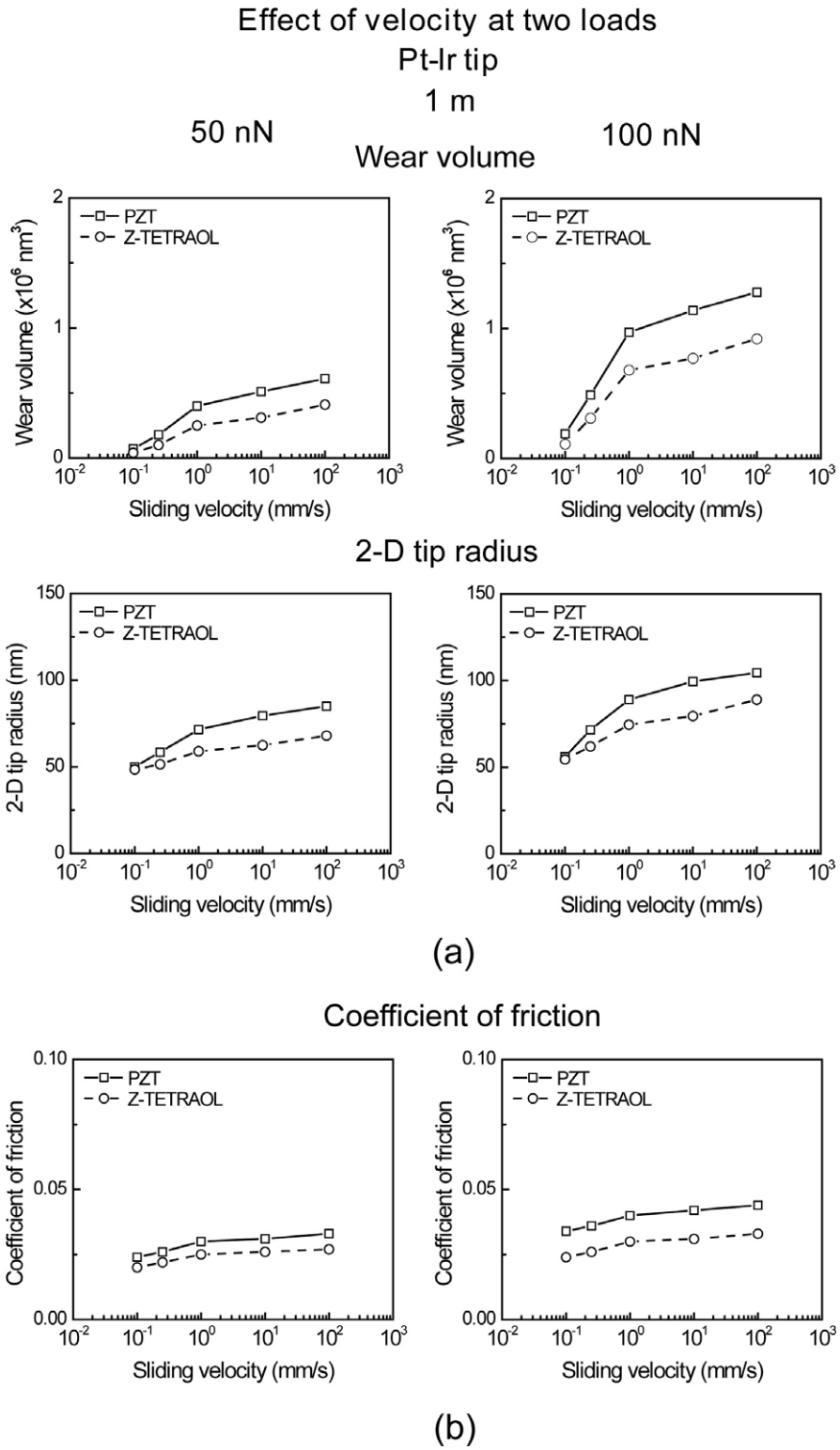

Figure 26. (a) Wear volumes, 2D tip radii and (b) coefficients of friction as a function of sliding velocity at two loads for Pt–Ir tips on the unlubricated and Z-TETRAOL-lubricated PZT films (Bhushan and Kwak 2008c).

the diverging wear volume and tip radius profiles indicate is that the formation of silicide, which is formed further in the Pt–Si interface, is instrumental in retarding the wear of the tip. As the actual thickness of the Pt layer on the tips of the Pt and Pt–Si probes cannot be evaluated in this experiment, we are using the tip wear data to conclude that both coatings are still affected beyond 1 m sliding. The Pt–Si data can be compared to that obtained for the various noble-metal-coated tips presented in section 4.3. Taking the data after 100 m sliding at 100 nN, the wear volumes of Pt–Si and Pt–Ir are 3.9×10^6 and 3.4×10^6 nm^3, respectively, indicating that Pt–Ir is more wear resistant than Pt–Si.

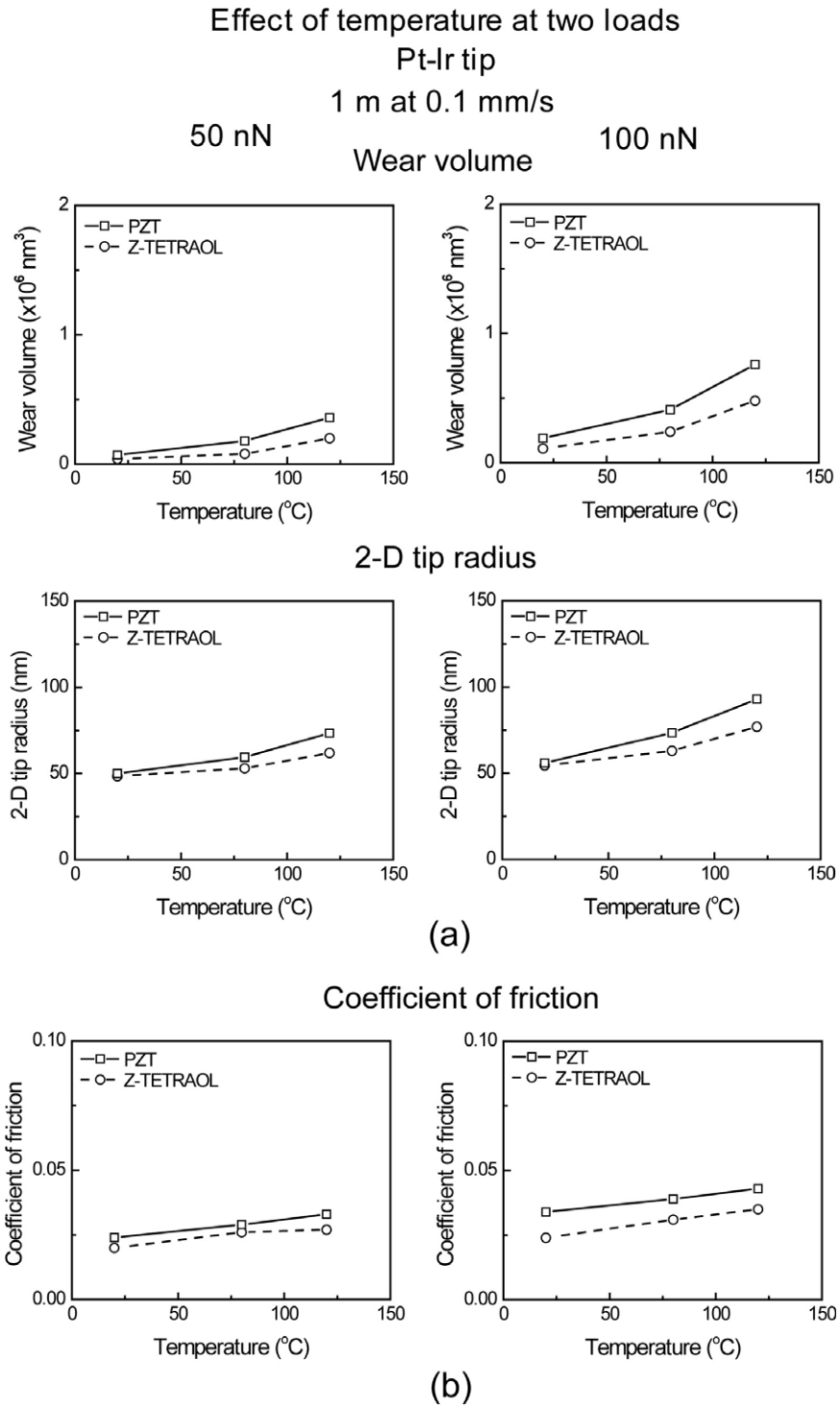

Figure 27. (a) Wear volumes, 2D tip radii and (b) coefficients of friction as a function of temperature at two loads for Pt–Ir tips on the unlubricated and Z-TETRAOL-lubricated PZT films (Bhushan and Kwak 2008c).

Figure 33(c) is a summary of the coefficient of friction of Pt–Si obtained by measuring the friction force at increasing normal loads before sliding and after sliding for 1, 10 and 100 m (Bhushan *et al* 2008a). The coefficient of friction values are lower than those obtained for Pt. For example, the value for Pt (Kwak and Bhushan 2008) and Pt–Si after sliding for a distance of 1 m are 0.073 and 0.034, respectively. Tip profiles provide evidence of an irregular worn surface, indicating abrasive wear, especially after long sliding distances. Brittle Pt-coated silicon asperities can fracture when sliding against the film surface. Particles would be produced by the fracture of asperities. These particles stay between the contacting surfaces and could accelerate the abrasive wear (Bhushan 2002, 2008, Tao and Bhushan 2006a). At high velocities, the impact of asperities becomes important and wear could be caused by periodic high velocity impact on the PZT film surface

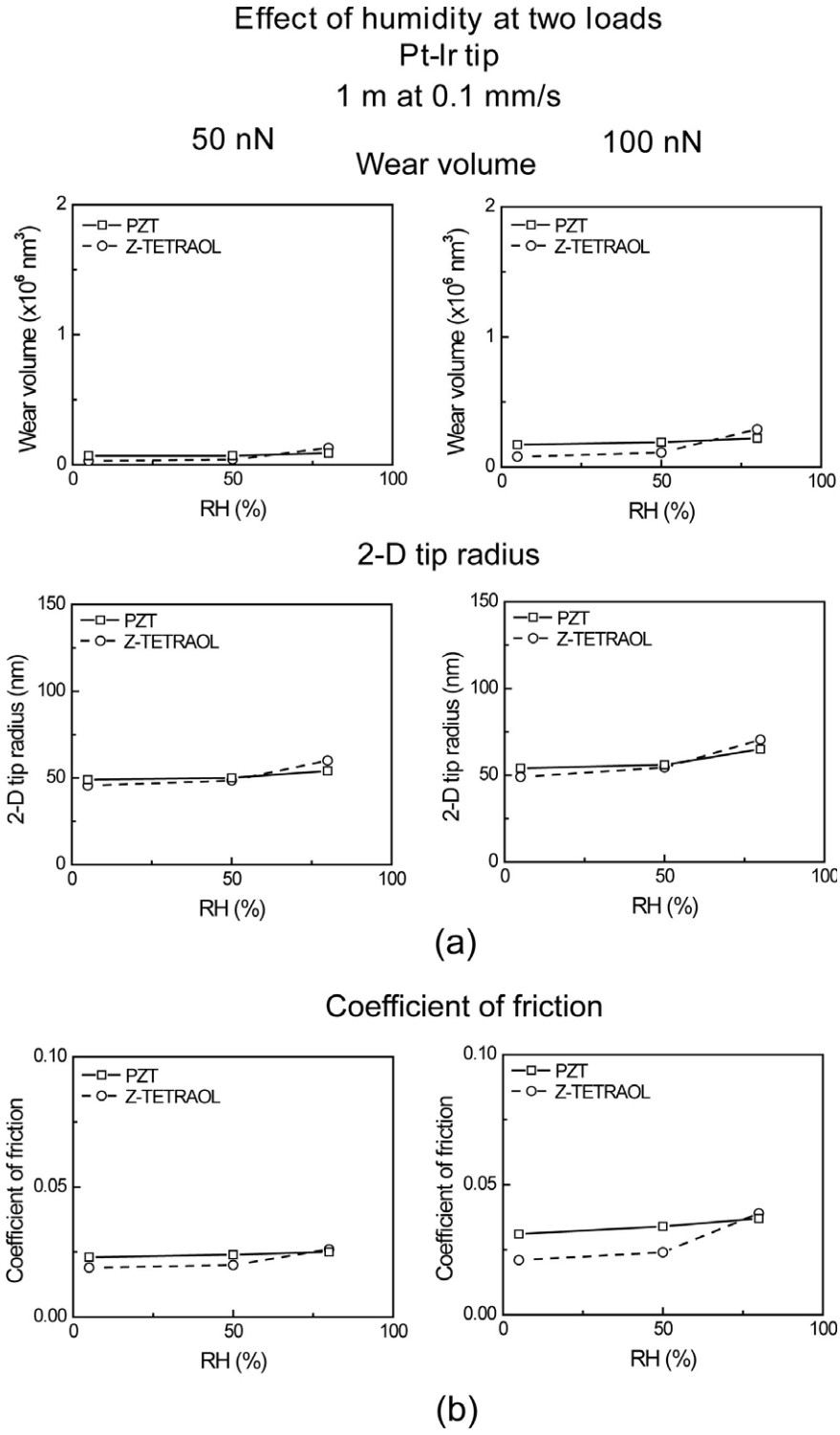

Figure 28. (a) Wear volumes, 2D tip radii and (b) coefficients of friction as a function of relative humidity at two loads for Pt–Ir tips on the unlubricated and Z-TETRAOL-lubricated PZT films (Bhushan and Kwak 2008c).

(Tambe and Bhushan 2005a, Tao and Bhushan 2007, Bhushan and Kwak 2007a, 2007b, Kwak and Bhushan 2008).

In addition to characterizing the probe tip, the tip shapes before and after sliding were imaged by SEM. Figure 34 shows SEM images of Pt and Pt–Si tips before the wear experiments and after sliding for 300 m at a load of 100 nN (Bhushan *et al* 2008a). The post-wear experimental images corroborate the 2D tip profiles in figure 33. From the SEM images of the worn tips, it can be deduced that the mechanism for tip wear is adhesive because the tip is plastically deformed. Blunting of the Pt–Si tip occurred to a lesser extent as observed in the 2D tip radius data in figure 33(b) (Bhushan *et al* 2008a). This can be attributed to the following reasons. Its H and E are higher than Pt, so less plastic deformation is expected. Also, Pt–Si

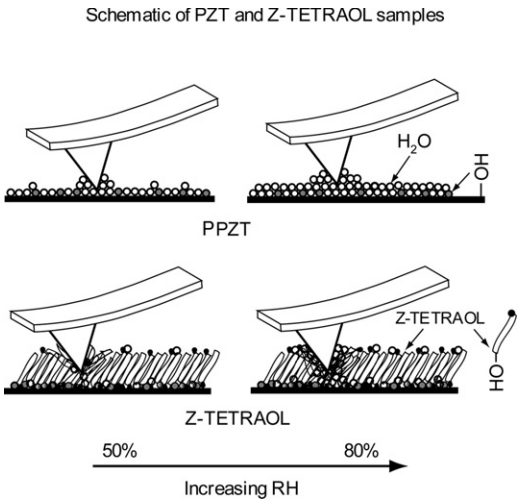

Figure 29. Schematic showing the change of meniscus between the AFM tip and the PZT samples, unlubricated and Z-TETRAOL-lubricated, with increasing RH (Bhushan and Kwak 2008c).

is brittle, so the generation of wear particles is more likely to occur, compared to blunting. In summary, from SEM imaging and tip profiling, as well as AFM imaging of the PZT, it was found that the Pt and Pt–Si tips exhibit adhesive and abrasive wear with some evidence of impact wear.

4.4.2. Nanomechanical characterization. Mechanical property analysis was also conducted by Bhushan *et al* (2008a) on the thermally treated coating to complement the wear experiments that they performed. Figure 35(a) is a summary of the hardness (H) and elastic modulus (E) of the Pt and Pt–Si films evaluated from nanoindentation studies (Bhushan *et al* 2008a). Measurements were taken at five different areas on the film surface, and the data is reproducible to within 10%. In figure 35(a), H and E as a function of contact depth are presented. Data points below a contact depth of 10 nm were truncated as they may be artificial. This is due to surface roughness as well as tip calibration limitations (Bhushan and Li 2003). The H and E, summarized in the bar plot in figure 35(b), are reported as the average of values from 10 to 30 nm contact depth (Bhushan *et al* 2008a). Beyond this depth, the hardness and elastic modulus of both films are expected to approach 13 and 180 GPa, respectively, which are the values for the underlying silicon substrate (Bhushan and Li 1997). The H and E of the film subjected to thermal treatment are 18 and 161 GPa, respectively, while the corresponding values for the untreated film are 15 and 152 GPa. This points to elemental composition changes in the thermally treated film, such as silicon diffusion into the Pt film, which could lead to platinum silicide formation. The extent of the mechanical property enhancement from silicide formation can vary widely and is influenced by the processing conditions used. For instance, a study on tantalum silicide formation was conducted where $TaSi_2$ films were deposited, then annealed at 700 °C (Sidorenko *et al* 2003). The silicide created had a hardness increase of 15–50% after annealing.

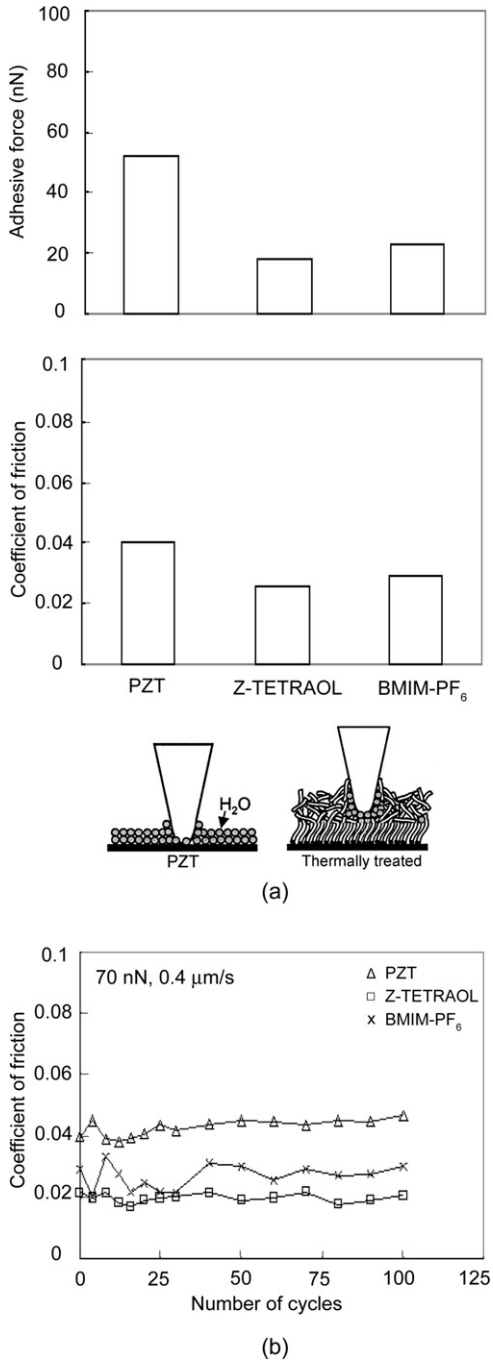

Figure 30. (a) Summary of the adhesive force and coefficient of friction and (b) durability data after 100 cycles using an Si_3N_4 tip (70 nN load, 0.4 μm s^{-1} sliding speed) for PZT, Z-TETRAOL and BMIM-PF_6 at room temperature (22 °C) and ambient air (45–55% RH). Data is reproducible to within 10%. Schematic in (a) shows the effect of chemical bonding treatment and meniscus formation between the AFM tip and sample surface on the adhesive and friction forces (Palacio and Bhushan 2008a).

The scratch behavior of Pt and Pt–Si is presented in figure 36(a) (Bhushan *et al* 2008a). The plot on the left-hand side shows the depth profile before, during and after a scratch, along with the coefficient of friction. The critical load to failure of the two films is summarized in figure 36(b). SEM images were taken at three areas: at the beginning of the

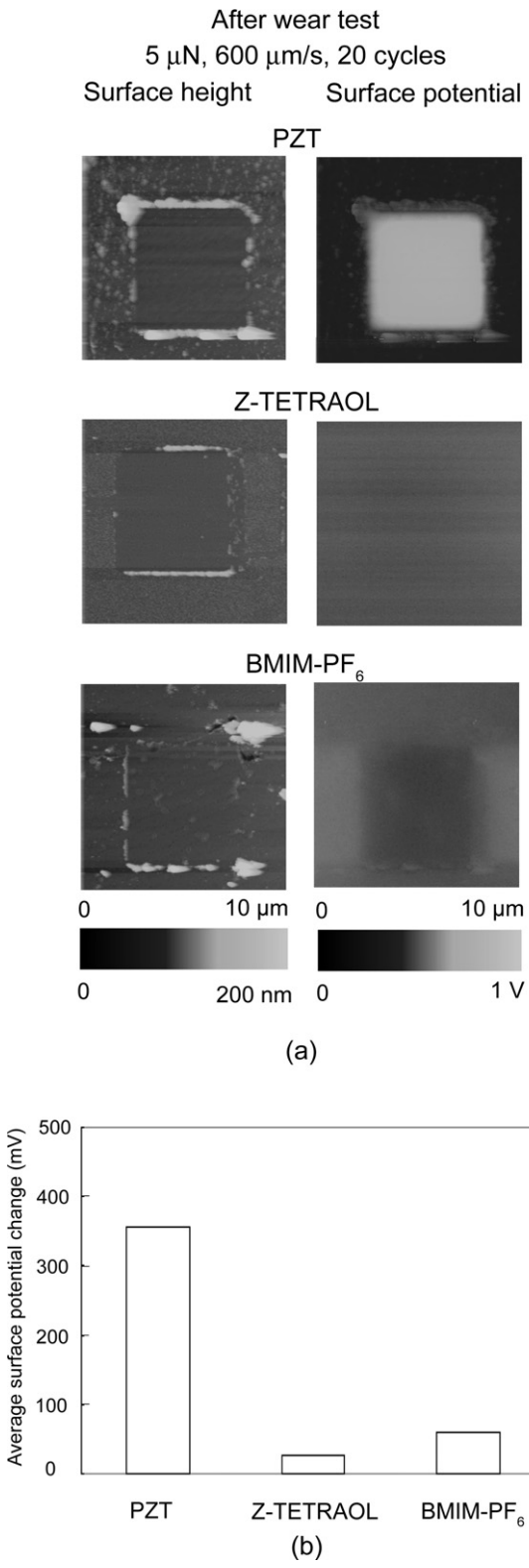

Figure 31. (a) Surface height and surface potential maps after wear tests using a diamond tip (5 μN load, 600 μm s^{-1} sliding speed, 20 cycles) and (b) bar chart showing surface potential change for PZT, Z-TETRAOL and BMIM-PF$_6$ (Palacio and Bhushan 2008a).

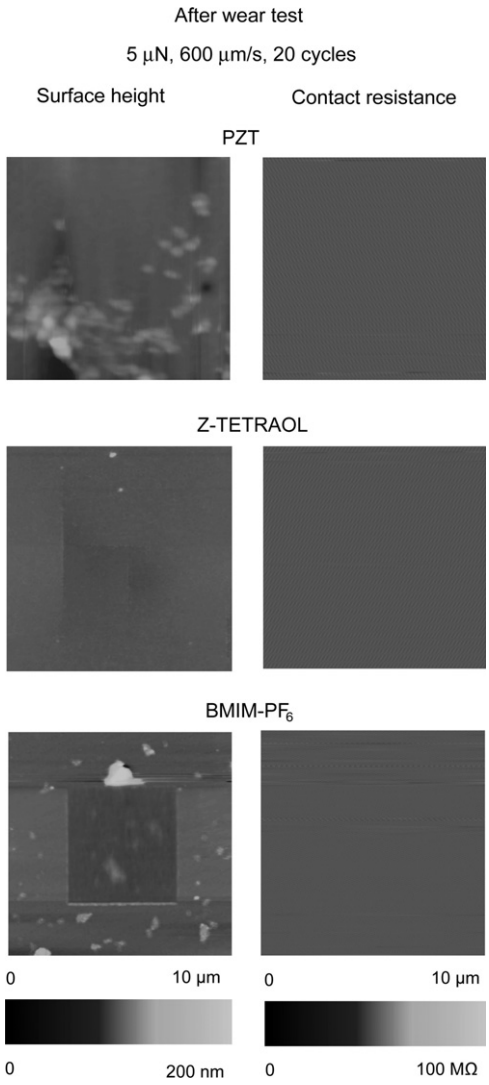

Figure 32. Surface height and contact resistance maps after wear tests using a diamond tip (5 μN load, 600 μm s^{-1} sliding speed, 20 cycles) for PZT, Z-TETRAOL and BMIM-PF$_6$. The trace of the wear scar is not observed in the resistance map, indicating that the lubricant was not fully removed from the test surface (Palacio and Bhushan 2008a).

scratch (indicated by 'A' on the friction profile), the middle of the scratch ('B') and towards the end of the scratch ('C'). The lack of sudden bursts in the surface profiles indicates that both the Pt and Pt–Si coatings have considerable scratch resistance. However, the SEM images of the two scratches are strikingly different. The scratch on the Pt film shows plowing and pile-up of material, indicating that plastic deformation was the main failure mechanism. Deformation is immediate, as evidenced by the visible track in the region A image. The corresponding region on Pt–Si is showing negligible damage. The scratch profile of the Pt–Si film shows discrete cracks and less pile-up, implying that the film fails mainly in a brittle manner. Bulk silicides are known to deform in a brittle manner (Bhushan and Gupta 1991, Sha and Yamabe-Mitarai 2006) and the scratch tracks shown in the SEM images of the Pt–Si sample confirm this. This accounts for the much higher critical load to failure (figure 36(b)) for the Pt–Si film compared to Pt.

4.4.3. Electrical and surface characterization. The electrical properties of the probe have to be characterized in order

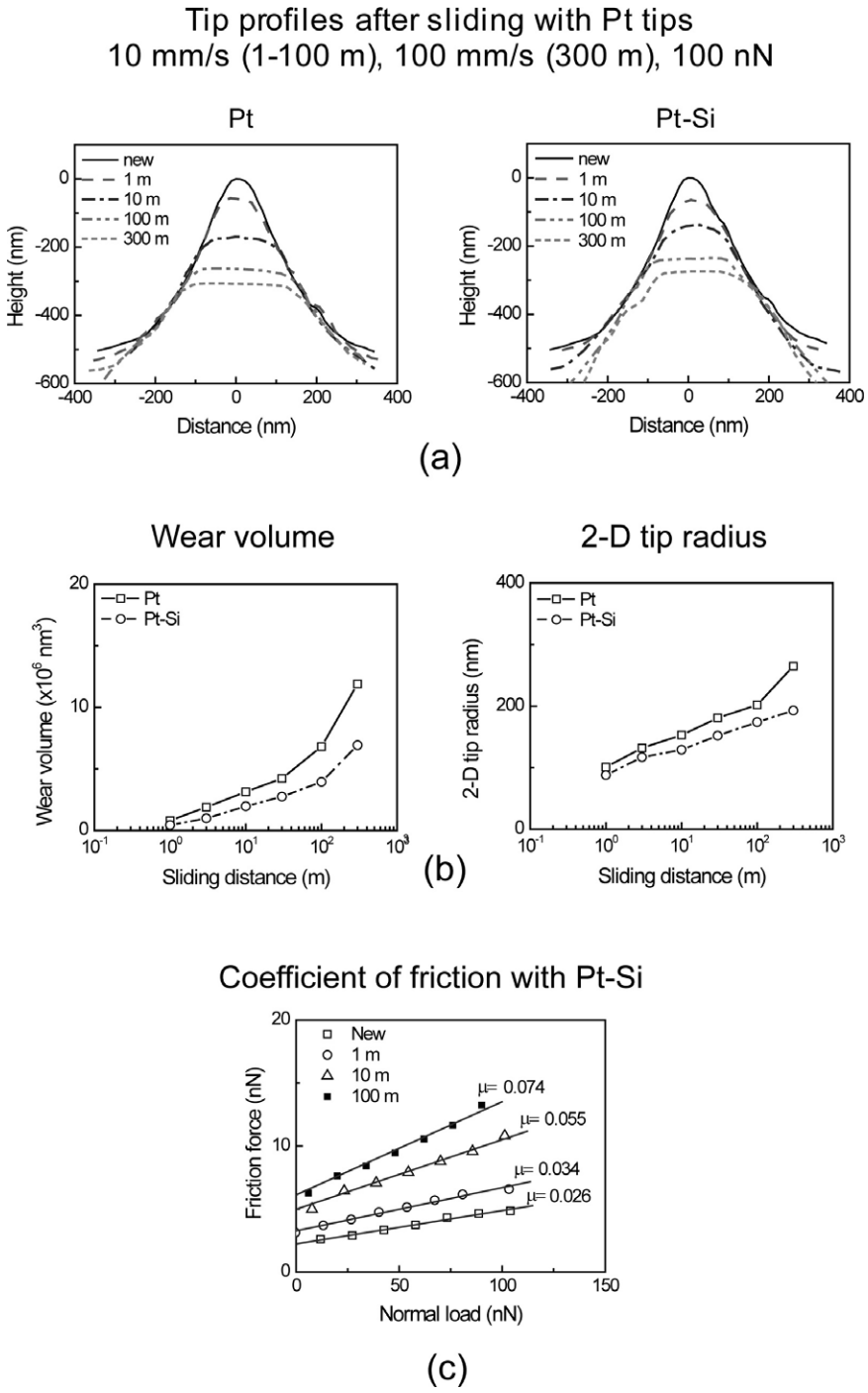

Figure 33. (a) Pt (untreated) and Pt–Si (thermally treated) tip profiles before and after 1, 10 and 100 m sliding at 10 mm s^{-1}, and 300 m sliding at 100 mm s^{-1} and at 100 nN on a PZT film. The solid curve corresponds to the virgin tip profile, (b) wear volumes and 2D tip radii after 1, 10 and 100 m sliding at 10 mm s^{-1}, and 300 m sliding at 100 mm s^{-1}, and (c) friction force as a function of normal load, obtained by measuring friction forces with a thermally treated Pt tip at increasing normal loads in a range of 1–80 nN after 1, 10 and 100 m sliding on the PZT film. The slopes of the linear fit are the coefficients of friction (Bhushan *et al* 2008a).

to evaluate the suitability of the thermally treated Pt film as a component of the ferroelectric data storage probe. To further investigate the difference between the untreated and thermally treated films, the electrical resistivity was measured by Bhushan *et al* (2008a) using a four-point probe, and the results are shown in figure 37. The thermal treatment increases the film resistivity from 17 to 34 $\mu\Omega$ cm. The measured resistivity of the thermally treated Pt film is in good agreement with the reported resistivity value for platinum silicide (as PtSi), which ranges from 30 to 38 $\mu\Omega$ cm (Murarka *et al* 1983, Naem 1988, Fujii *et al* 1991, Conforto and Schmid 2001, Zhang *et al* 2006). Aside from confirming that platinum silicide formation took place, this implies that the silicide formed is present as PtSi and not as Pt_2Si since the resistivity

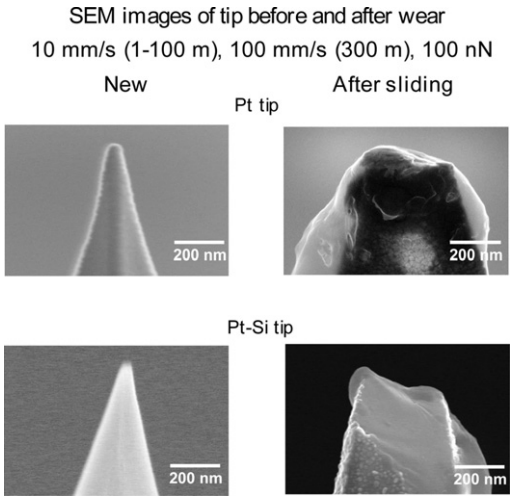

Figure 34. SEM images of a virgin tip and tips obtained after 300 m sliding at 100 nN for the Pt (untreated) and Pt–Si (thermally treated) tips (Bhushan *et al* 2008a).

of the latter is slightly lower (26 $\mu\Omega$ cm) (Zhang *et al* 2006). This further strengthens the hypothesis that the observed improvement in the mechanical properties and wear resistance is the result of platinum silicide formation. In addition, the results show that the platinum silicide film remains conductive, which is a necessary requirement for implementation of the thermal treatment process in probe-based ferroelectric data recording.

Auger electron spectroscopy was conducted by Bhushan *et al* (2008a) on the thermally treated Pt film to examine the elemental distribution on the surface and near-surface. The Auger spectrum of the surface, shown in figure 38(a), indicates the presence of Si and Pt. The Si peaks at 82 and 1615 eV are due to LMM and KLL transitions, respectively, while the two Pt peaks at 1975 and 2020 eV are both due to MNN transitions. Carbon and oxygen are always detected as they are typical contaminants (Feldman and Mayer 1986). The elemental composition as a function of depth was also obtained by slowly sputtering the surface and performing the analysis in every step. The Si concentration data at the surface are suspect and can be due to the presence of contaminants. After sputtering for a minute, the Pt to Si concentration is about 20:1. This denotes that the Si was able to diffuse through the grain boundaries in the Pt film. There is a spike in the concentration of oxygen in the near-surface (approx. 4 min sputter time), which implies that O is more than a surface contaminant; SiO_2 formation may have occurred at this depth. One key finding from this experiment is that beyond 12 nm depth (4 min sputter time), the concentration of Pt slowly decreases while that of Si increases correspondingly. At about 15 nm depth, the atomic concentrations of Pt and Si are both about 50%. These observations imply that Si is diffusing through the Pt film and may lead to the formation of compounds such as platinum silicide. As discussed in section 3, the measured resistivity of this film corresponds to the value for PtSi. As shown in the depth profile in figure 38(b), the Pt atomic concentration approaches zero and Si approaches 100% after

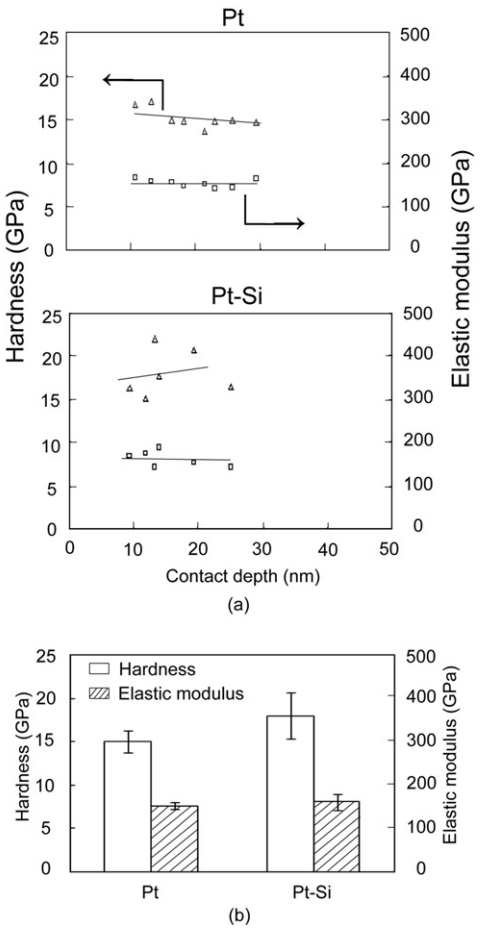

Figure 35. (a) Hardness and elastic modulus of the Pt (untreated) and Pt–Si (thermally treated) films as a function of contact depth greater than 10 nm, and (b) bar plot summarizing hardness and elastic modulus values. The H and E were taken as the average of values from 10 to 30 nm contact depth. The error bars represent $\pm 1\sigma$ (Bhushan *et al* 2008a).

sputtering for about 10 min. This indicates that the substrate is exposed at this point and the thermally treated 30 nm thick film has been fully removed. Therefore, the Auger analysis was instrumental in confirming platinum silicide formation and in identifying that the silicide layer is present at the lower half of the film closer to the film–substrate interface. By using a similar thermal treatment technique, the formation of platinum silicide has been reported by various groups (Murarka *et al* 1983, Conforto and Schmid 2001, Yin *et al* 2005) and their composition confirmed using various characterization methods such as x-ray diffraction (XRD), x-ray photoelectron spectroscopy (XPS) and transmission electron microscopy (TEM). The Auger profile obtained on this sample, along with the resistivity data and previous experimental reports, all support the formation of platinum silicide on AFM tips with Pt thin films subjected to *in situ* thermal treatment processing.

4.5. Summary

Wear studies at sliding velocities of 10 and 100 mm s^{-1} have been conducted on Pt-, Au–Ni-, Pt–Ir-and Pt–Ni-coated tips

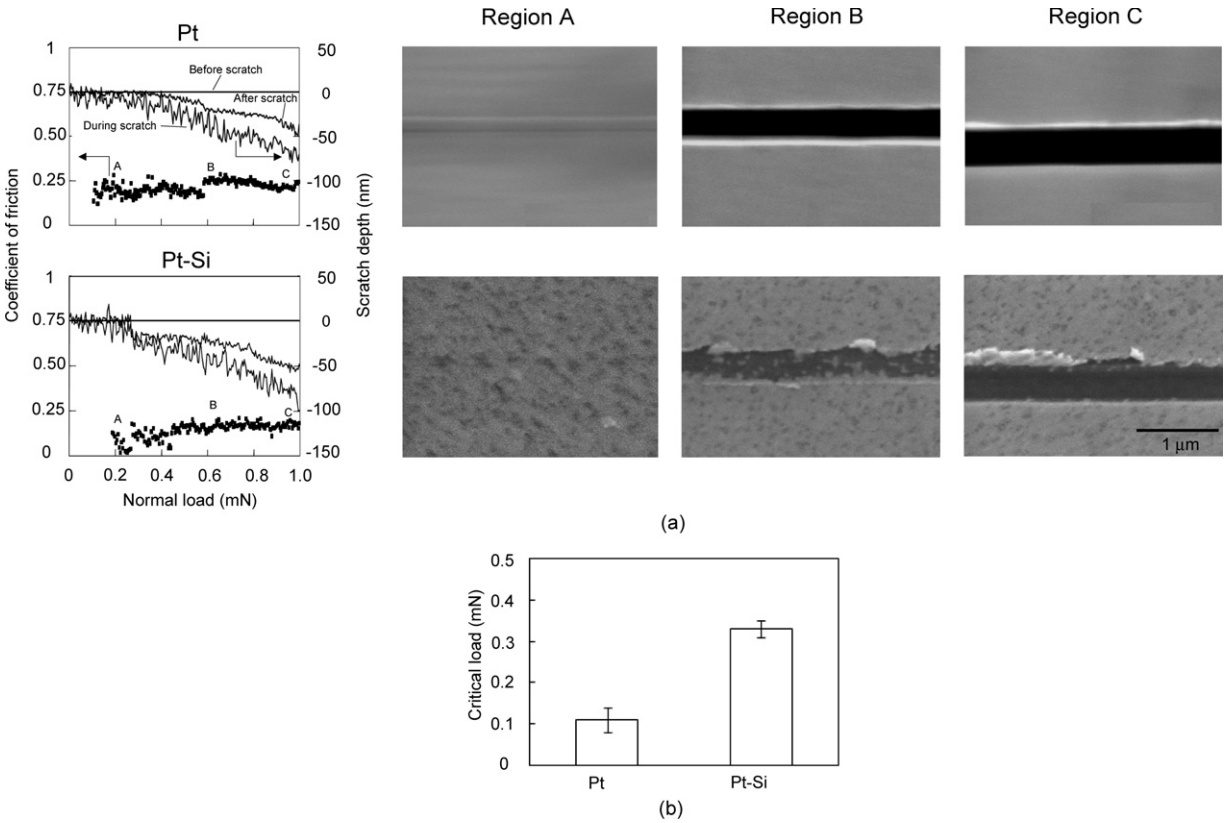

Figure 36. (a) Scratch depth profile and coefficient of friction as a function of increasing normal load for Pt (untreated) and Pt–Si (thermally treated). SEM images were taken at three regions: at the beginning of the scratch ('A'), at the middle of the scratch ('B') and at the end of the scratch ('C'), and (b) bar plot summarizing the critical load to failure of the surface from scratch testing. The error bars represent $\pm 1\sigma$ (Bhushan *et al* 2008a).

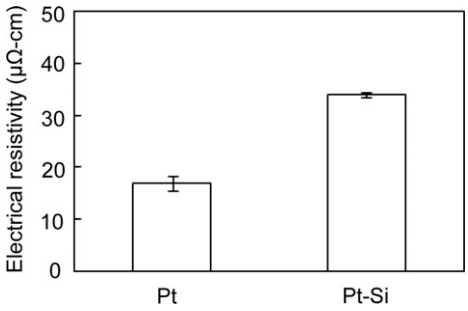

Figure 37. Bar plot summarizing the measured electrical resistivity of the Pt (untreated) and Pt–Si (thermally treated) films. The error bars represent $\pm 1\sigma$ (Bhushan *et al* 2008a).

sliding on PZT film, a ferroelectric medium for a total sliding distance of 300 m. The Au–Ni and Pt–Ir tips are shown to exhibit less wear compared to the Pt tips, with Pt–Ni of intermediate values. The tip wear mechanism is primarily adhesive and abrasive wear, with some evidence of impact wear. The coefficient of friction increases sliding wear.

Two lubricants, Z-TETRAOL and BMIM-PF_6, have been deposited on PZT films. It was reported that adhesion, friction and wear for the Pt–Ir tips against the Z-TETRAOL-lubricated PZT film are the lowest, followed by the BMIM-PF_6-lubricated PZT film. From AFM images, the wear scars of PZT against the Pt–Ir tip show plowing of PZT material and pile-up in the wear tracks, which is indicative of adhesive wear. From the SEM images of the worn tips, it is also deduced that the mechanism for tip wear is adhesive because the tip is plastically deformed. Tip profiles provide evidence of an irregular worn surface, indicating abrasive wear, especially after long sliding distances. Particles produced by the fracture of asperities stay between the contacting surfaces and could accelerate the abrasive wear.

Based on studies on the effect of the velocity on tip wear, the sliding velocity appears to play a significant role. Wear and friction increase as a logarithm of velocity in the lower velocity range, which is based on the thermally activated stick–slip mechanism. The wear increases slowly in the higher velocity range and is believed to be a combination of adhesive, abrasive and impact wear. From the high temperature experiments, wear and friction for both unlubricated and lubricated PZT increase with an increase in the sample temperature. The increase is believed to be associated with the degradation of the mechanical properties of PZT. The tip sliding on the Z-TETRAOL-lubricated PZT exhibited lower wear volume and friction than those on unlubricated surfaces at a given temperature. Wear and friction increase with an increase in the relative humidity for both samples. At higher relative humidity, a thicker surface water layer is expected to develop, which develops meniscus forces responsible for an increase in wear volume and friction. For the Z-TETRAOL-lubricated PZT, wear and friction increase with relative humidity with

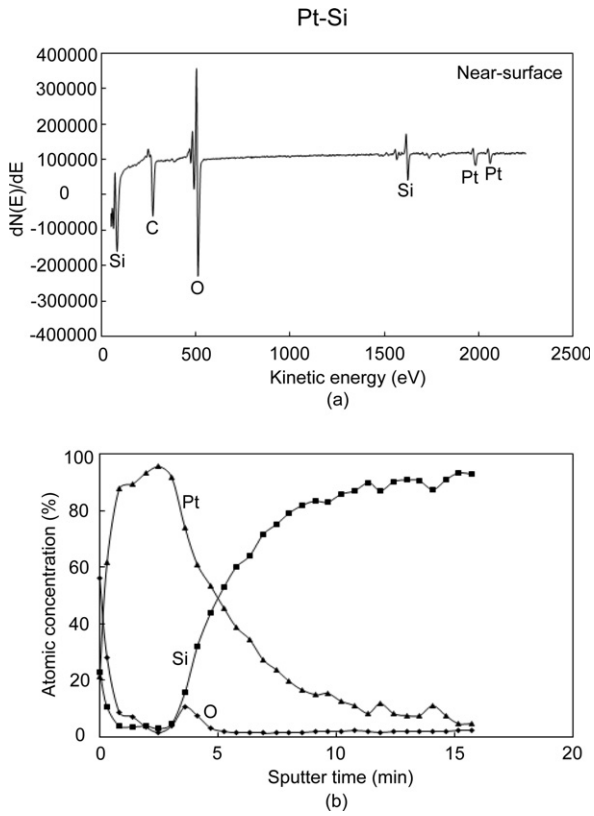

Figure 38. (a) Auger spectrum of the Pt–Si (thermally treated) film surface and (b) Auger depth profile showing the atomic concentrations of O, Pt and Si as a function of sputter time. The sputter rate is 3 nm min^{-1}, which is based on a depth profile on a silicon nitride thin film standard (Bhushan *et al* 2008a).

a larger rate of increase at relative humidity larger than 50% RH because of aggregation of water molecules with mobile lubricant.

Silicide formation has been successfully accomplished by thermal treatment of a Pt film on a silicon AFM probe. From mechanical characterization, it was demonstrated that this Pt–Si film has better hardness and elastic modulus, and its scratch deformation behavior is primarily brittle. Elemental analysis using Auger electron spectroscopy reveals the presence of equal amounts of Pt and Si in the near-surface of the thermally treated Pt film, indicating that platinum silicide formation occurred. Electrical resistivity measurements confirm silicide formation and show that the thermally treated film remains conducting. High velocity sliding experiments on PZT show that both Pt–Si and Pt tips exhibit adhesive and abrasive wear with some evidence of impact wear, and that the Pt–Si tip is more wear resistant compared to Pt. The thermal treatment makes these platinum silicide probes wear resistant, electrically conducting and therefore suitable for probe-based nonvolatile ferroelectric data storage applications. This study demonstrates how a compound thin film on AFM tips can be produced by thermal treatment *in situ*.

5. Conclusion

Nanotribological and nanomechanical characterization studies carried out on materials used for probe-based phase change and ferroelectric data recording technologies are reviewed in this paper. In both of these technologies, probe tip wear is strongly affected by temperature and sliding velocity. Aside from commonly observed adhesive and abrasive wear, thermally activated stick–slip is a dominant mechanism. For phase change recording, the tribochemical reaction of the DLC film is another important wear mechanism. In ferroelectric data recording, both the probe tip and the PZT medium exhibit wear. Various commercial noble-metal-coated tips were studied, and it was found that the Pt–Ir tip is more wear resistant than Pt and the other tips. A Pt tip that was thermally treated to form platinum silicide also exhibited better wear resistance compared to Pt. These studies advance the understanding of the physics of adhesion, friction and wear of AFM probes, and are not only applicable to probe-based data recording technology, but also to the development of reliable AFM probes in general.

References

Ahn C H, Tybell T, Antognazza L, Char Z, Hammond R H, Beasley M R, Fischer O and Triscone J M 1997 Local, nonvolatile writing of epitaxial $Pb(Zr_{0.52}Ti_{0.48})O_3/SrRuO_3$ heterostructures *Science* **276** 1100–3

Arimoto Y and Ishiwara H 2004 Current status of ferroelectric random-access memory *MRS Bull.* **29** 823–6

Baker S and Nix W D 1994 Mechanical properties of compositionally modulated Au–Ni thin films: nanoindentation and microcantilever deflection experiments *J. Mater. Res.* **9** 3131–44

Barrett R C and Quate C F 1991 Charge storage in a nitride–oxide–silicon medium by scanning capacitance microscopy *J. Appl. Phys.* **70** 2725–33

Bertram H N and Williams M 2000 SNR and density limit estimates: a comparison of longitudinal and perpendicular recording *IEEE Trans. Magn.* **36** 4–9

Betzig E, Trautman J K, Wolfe R, Gyorgy E M, Finn P L, Kryder M H and Chang C H 1992 Near-field magneto-optics and high density data storage *Appl. Phys. Lett.* **61** 142–4

Bhushan B 1996 *Tribology and Mechanics of Magnetic Storage Devices* 2nd edn (New York: Springer)

Bhushan B 1999a Chemical, mechanical, and tribological characterization of ultra-thin and hard amorphous carbon coatings as thin as 3.5 nm: recent developments *Diamond Relat. Mater.* **8** 1985–2015

Bhushan B 1999b *Handbook of Micro/Nanotribology* 2nd edn (Boca Raton, FL: CRC Press)

Bhushan B 2002 *Introduction to Tribology* (New York: Wiley)

Bhushan B 2008 *Nanotribology and Nanomechanics—An Introduction* 2nd edn (Heidelberg: Springer)

Bhushan B and Gupta B K 1991 *Handbook of Tribology: Materials, Coatings and Surface Treatments* (New York: McGraw-Hill)

Bhushan B, Kulkarni A V, Bonin W and Wyrobek J 1996 Nano/picoindentation measurement using a capacitance transducer system in atomic force microscopy *Phil. Mag.* **74** 1117–28

Bhushan B and Kwak K J 2007a Platinum-coated probes sliding at up to 100 mm s^{-1} against coated silicon wafers for AFM probe-based recording technology *Nanotechnology* **18** 345504

Bhushan B and Kwak K J 2007b Velocity dependence of nanoscale wear in atomic force microscopy *Appl. Phys. Lett.* **91** 163113

Bhushan B and Kwak K J 2008a Effect of temperature on nanowear of platinum-coated probes sliding against coated silicon wafers for probe-based recording technology *Acta Mater.* **56** 380–6

Bhushan B and Kwak K J 2008b Noble metal-coated probes sliding at up to 100 mm s^{-1} against PZT films for AFM probe-based ferroelectric recording technology, (invited) *J. Phys.: Condens. Matter* **20** 225013

Bhushan B and Kwak K J 2008c The role of lubricants, scanning velocity, and environment on adhesion, friction and wear of Pt–Ir coated probes for atomic force microscope probe-based ferroelectric recording technology *J. Phys.: Condens. Matter* **20** 325240

Bhushan B and Li X 1997 Micromechanical and tribological characterization of doped single-crystal silicon and polysilicon films for microelectromechanical systems devices *J. Mater. Res.* **12** 54–63

Bhushan B and Li X 2003 Nanomechanical characterization of solid surfaces and thin films *Int. Mater. Rev.* **48** 125–64

Bhushan B, Palacio M and Kinzig B 2008a AFM-based nanotribological and electrical characterization of ultrathin wear-resistant ionic liquid films *J. Colloids Interface Sci.* **317** 275–87

Bhushan B, Palacio M and Kwak K J 2008b Thermally-treated Pt-coated silicon AFM tips for wear resistance in ferroelectric data storage *Acta Mater.* at press

Blom P W M, Wolf R M, Cillessen J F M and Krijin M P C M 1994 Ferroelectric Schottky diode *Phys. Rev. Lett.* **73** 2107–10

Callister W D 2000 *Materials Science and Engineering: An Introduction* 5th edn (New York: Wiley)

Carda-Broch S, Berthod A and Armstrong D W 2003 Solvent properties of the 1-butyl-3-methylimidazolium hexafluorophosphate ionic liquid *Anal. Bioanal. Chem.* **375** 191–9

Chung K H, Lee Y H, Kim Y T, Kim D E, Yoo J and Hong S 2007 Nano-tribological characteristics of PZT thin film investigated by atomic force microscopy *Surf. Coat. Technol.* **201** 7983–91

Conforto E and Schmid P E 2001 Pt–Si reaction through interfacial native silicon oxide layers *Phil. Mag.* A **81** 61–82

Conoci S, Petralia S, Samorì P, Raymo F M, Bella S D and Sortino S 2006 Optically transparent, ultrathin Pt films as versatile metal substrates for molecular optoelectronics *Adv. Funct. Mater.* **16** 1425–32

Cooper E B, Manalis S R, Fang H, Dai H, Matsumoto K, Minne S C, Hunt T and Quate C F 1999 Terabit-per-square-inch data storage with the atomic force microscope *Appl. Phys. Lett.* **75** 3566–8

Coughlin T and Handy J 2006 Flash vs. hard drives: the battle intensifies *Solid State Technol.* **49** S14–8

Davis J R 1998 *Metals Handbook: Desk Edition* 2nd edn (Materials Park, OH: ASM International)

Fang T H, Jian S R and Chuu D S 2003 Nanomechanical properties of lead zirconate titanate thin films by nanoindentation *J. Phys.: Condens. Matter* **15** 5253–9

Fazio A 2004 Flash memory scaling *MRS Bull.* **29** 814–7

Feldman L C and Mayer J W 1986 *Fundamentals of Surface and Thin Film Analysis* (Englewood Cliffs, NJ: Prentice-Hall)

Field J E (ed) 1992 *The Properties of Natural and Synthetic Diamond* (London: Academic)

Franke K, Besold J, Haessler W and Seegebarth C 1994 Modification and detection of domains on ferroelectric PZT films by scanning force microscopy *Surf. Sci.* **302** L283–8

Frez C, Diebold G J, Tran C D and Yu S 2006 Determination of thermal diffusivities, thermal conductivities and sound speed of room-temperature ionic liquids by the transient grating technique *J. Chem. Eng. Data* **51** 1250–5

Fujii K, Kanaya H, Kumagai Y, Hasegawa F and Yamaka E 1991 Low-temperature formation of the PtSi layer by codeposition of Pt and Si in a molecular beam epitaxy system *Japan. J. Appl. Phys.* **30** L455–7

Gidon S, Lemonnier O, Rolland B, Dressler C and Samson Y 2004 Electrical probe storage using joule heating in phase change media *Appl. Phys. Lett.* **85** 6392–4

Gruverman A, Auciello O and Tokumoto H 1996 Scanning force microscopy for the study of domain structure in ferroelectric thin films *J. Vac. Sci. Technol.* B **14** 602–5

Guthner P and Dransfeld K 1992 Local poling of ferroelectric polymers by scanning force microscopy *Appl. Phys. Lett.* **61** 1137–9

Hidaka T, Maruyama T, Saitoh M, Mikoshiba N, Shimizu M, Shiosaki T, Willis L A, Hiskes R, Dicarolis S A and Amano J 1996 Formation and observation of 50 nm polarized domains in $PbZr_{1-x}Ti_xO_3$ thin film using scanning probe microscope *Appl. Phys. Lett.* **68** 2358–9

Hultgren R, Orr R, Anderson P and Kelly K 1963 *Selected Values of Thermodynamic Properties of Metals and Alloys* (New York: Wiley)

Kabo G J, Blokhin A V, Paulechka Y U, Kabo A J, Shymanovich M P and Magee J W 2004 Thermodynamic properties of 1-butyl-3-methylimidazolium hexafluorophosphate in the condensed state *J. Chem. Eng. Data* **49** 453–61

Kado H and Tohda T 1995 Nanometer-scale recording on chalcogenide films with an atomic force microscope *Appl. Phys. Lett.* **66** 2961–2

Kalinin S V and Bonnell D A 2002 Imaging mechanism of piezoresponse force microscopy of ferroelectric surfaces *Phys. Rev.* B **65** 125408

Kinzig B J and Sutor P 2005 Ionic liquids: novel lubrication for air and space *Phase I Final Report for AFOSR/NL* (Lenexa, KS.: Surfaces Research and Applications)

Kozlov A, Chang C F, Taylor R D, Franz L R and Leone E A 2000 Wear-resistant spark plug electrode tip containing platinum alloys, spark plug containing the wear-resistant tip, and method of making same *US Patent Specification* 6071163

Kwak K J and Bhushan B 2008 Platinum-coated probes sliding at up to 100 mm s^{-1} against lead zirconate titanate films for atomic force microscopy probe-based ferroelectric recording technology *J. Vac. Sci. Technol.* A **26** 783–93

Li X and Bhushan B 2001 Micro/nanomechanical and tribological studies of bulk and thin-film materials used in magnetic recording heads *Thin Solid Films* **398/399** 313–9

Liu H and Bhushan B 2003 Nanotribological characterization of molecularly thick lubricant films for applications to MEMS/NEMS by AFM *Ultramicroscopy* **97** 321–40

Maimon J, Spall E, Quinn R and Schnur S 2001 Chalcogenide-based non-volatile memory technology *Proc. IEEE Aerosp. Conf.* **5** 2289–94

Mamin H J and Rugar D 1992 Thermomechanical writing with an atomic force microscope tip *Appl. Phys. Lett.* **61** 1003–5

Martin Y, Abraham D W and Wickramasinghe H K 1988 High-resolution capacitance measurement and potentiometry by force microscopy *Appl. Phys. Lett.* **52** 1103–5

Merck Ionic Liquids Database 2004 Darmstadt, Germany, also http://ildb.merck.de/ionicliquids/en/startpage.htm

Mihara T, Watanabe H and Araujo C A P 1994 Polarization fatigue characteristics of sol–gel ferroelectric $Pb(Zr_{0.4}Ti_{0.6})O_3$ thin-film capacitors *Japan. J. Appl. Phys.* **33** 3996–4002

Morimoto K, Uematsu A, Sawai S, Hisano K and Yamamoto T 2003 Simultaneous measurement of thermophysical properties and dielectric properties of PZT-based ferroelectric ceramics by thermal radiation calorimetry *Int. J. Thermophys.* **24** 821–35

Murarka S P, Kinsbron E, Fraser D B, Andrews J M and Lloyd E J 1983 High temperature stability of ptsi formed by reaction of metal with silicon or by cosputtering *J. Appl. Phys.* **54** 6943–51

Naem A A 1988 Platinum silicide formation using rapid thermal processing *J. Appl. Phys.* **64** 4161–7

Nakamura J, Miyamoto M, Hosaka S and Koyanagi H 1995 High density thermomagnetic recording method using a scanning tunneling microscope *J. Appl. Phys.* **77** 779–81

Nonnenmacher M, O'Boyle M P and Wickramasinghe H K 1991 Kelvin probe force microscopy *Appl. Phys. Lett.* **58** 2921–3

Ohkubo T, Kishigami J, Yanagisawa K and Kaneko R 1991 Submicron magnetizing and its detection based on the point magnetic recording concept *IEEE Trans. Magn.* **27** 5286–8
Ovshinsky S R 1968 Reversible electrical switching phenomena in disordered structures *Phys. Rev. Lett.* **21** 1450–3
Palacio M and Bhushan B 2007 Surface potential and resistance measurements for detecting wear of chemically-bonded and unbonded molecularly-thick perfluoroether lubricant films using atomic force microscopy *J. Colloid Interface Sci.* **315** 261–9
Palacio M and Bhushan B 2008a Nanotribological and nanomechanical properties of lubricated PZT thin films for ferroelectric data storage applications *J. Vac. Sci. Technol.* A **26** 768–76
Palacio M and Bhushan B 2008b Nanomechanical and nanotribological characterization of noble metal-coated AFM tips for probe-based ferroelectric data recording *Nanotechnology* **19** 105705
Palacio M and Bhushan B 2008c Ultrathin wear-resistant ionic liquid films for novel MEMS/NEMS applications *Adv. Mater.* **20** 1194–8
Reich R A, Stewart P A, Bohaychick J and Urbanski J A 2003 Base oil properties of ionic liquids *Lubr. Eng.* **49** 16–21
Richter H J 2007 The transition from longitudinal to perpendicular recording *J. Phys. D: Appl. Phys.* **40** R149–77
Roelofs A, Bottger U, Waser R, Schlaphof F, Trogisch S and Eng L M 2000 Differentiating 180° and 90° switching of ferroelectric domains with three-dimensional piezoresponse force microscopy *Appl. Phys. Lett.* **77** 3444–6
Rooney D, Negrotti D, Byassee T, Macero D, Chaiken J and Vastag B 1990 Use of laser-directed chemical vapor deposition to fabricate durable, optically transparent, platinum thin film electrode *J. Electrochem. Soc.* **137** 1162–6
Rottmayer R E, Batra S, Buechel D, Challener W A, Hohlfeld J, Kubota Y, Li L, Lu B, Mihalcea C, Mountfield K, Pelhos K, Peng C, Rausch T, Seigler M A, Weller D and Yang X M 2006 Heat-assisted magnetic recording *IEEE Trans. Magn.* **42** 2417–21
Ruan J and Bhushan B 1994 Atomic-scale friction measurements using friction force microscopy: part I—General principles and new measurement techniques *ASME J. Tribol.* **116** 378–88
Saurenbach F and Terris B D 1990 Imaging of ferroelectric domain walls by force microscopy *Appl. Phys. Lett.* **56** 1703–5
Setter N, Damjanovic D, Eng L, Fox G, Gevorgian S, Hong S, Kingon A, Kohlstedt H, Park N Y, Stephenson G B, Stolichnov I, Taganstev A K, Taylor D V and Yamada T 2006 Ferroelectric thin films: review of materials, properties and applications *J. Appl. Phys.* **100** 051606
Sha J B and Yamabe-Mitarai Y 2006 Phase and microstructural evolution of Ir–Si binary alloys with FCC/silicide structure *Intermetallics* **14** 672–84
Shi L and Majumdar A 2002 Thermal transport mechanisms at nanoscale point contacts *J. Heat Trans.* **124** 329–37
Shin H, Hong S, Moon J and Jeon J U 2002 Read/write mechanisms and data storage system using atomic force microscopy and MEMS technology *Ultramicroscopy* **91** 103–10
Shin H, Lee K M, Moon W K, Jeon J U, Lim G, Pak Y E, Park J H and Yoon K H 2000 An application of polarized domains in ferroelectric thin films using scanning probe microscope *IEEE Trans. Ultrason. Ferroelectr. Freq. Control* **47** 801–07
Sidorenko S I, Makogon Y N, Beke D L, Csik A, Dub S N, Pavlova E P and Zelenin O V 2003 Formation of nanocrystalline structure of $TaSi_2$ films on silicon *Powder Metall. Metal Ceram.* **42** 14–8
Strand D 2005 Ovonics: from science to products *J. Optoelec. Adv. Mater.* **7** 1679–90
Su C, Huang L, Kjoller K and Babcock K 2003 Studies of tip wear processes in tapping mode atomic force microscopy *Ultramicroscopy* **97** 135–44
Tambe N S and Bhushan B 2005a Friction model for the velocity dependence of nanoscale friction *Nanotechnology* **16** 2309–24
Tambe N S and Bhushan B 2005b Nanoscale friction-induced phase transformation of diamond-like carbon *Scr. Mater.* **52** 751–5
Tao Z and Bhushan B 2005 Bonding, degradation and environmental effects on novel perfluoroether lubricants *Wear* **259** 1352–61
Tao Z and Bhushan B 2006a Surface modification of AFM silicon probes for adhesion and wear reduction *Tribol. Lett.* **21** 1–16
Tao Z and Bhushan B 2006b Surface modification of AFM Si_3N_4 probes for adhesion/friction reduction and imaging improvement *ASME J. Tribol.* **128** 865–75
Tao Z and Bhushan B 2006c A new technique for studying nanoscale friction at sliding velocities up to 200 mm s^{-1} using atomic force microscope *Rev. Sci. Instrum.* **77** 103705
Tao Z and Bhushan B 2007 Velocity dependence and rest time effect on nanoscale friction of ultrathin films at high sliding velocities *J. Vac. Sci. Technol.* A **25** 1267–74
Tybell T, Paruch P, Giamarchi T and Triacone J-M 2002 Domain wall creep in epitaxial ferroelectric $Pb(Zr_{0.2}Ti_{0.8})O_3$ thin films *Phys. Rev. Lett.* **89** 097601
Verdyan A, Soifer Y M, Azoulay J, Rabkin E and Kazakevich M 2005 Nanohardness and crack resistance of HTS YBCO thin films *IEEE Trans. Appl. Supercond.* **15** 3585–7
Vettiger P, Brugger J, Despont M, Dreschler U, Durig U, Haberle W, Lutwyche M, Rothuizen H, Stuz R, Widmer R and Binnig G 1999 Ultrahigh density, high data rate NEMS-based AFM data storage system *Microelectron. Eng.* **46** 11–7
Villarrubia J S 1994 Morphological estimation of tip geometry for scanned probe microscopy *Surf. Sci.* **321** 287–300
Wang H, Lu Q, Ye C, Liu W and Cui Z 2004 Friction and wear behaviors of ionic liquid of alkylimidazolium hexafluorophosphates as lubricants for steel/steel contacts *Wear* **256** 44–8
Wright C D, Armand M and Aziz M M 2006 Terabit-per-square-inch data storage using phase change media and scanning electrical nanoprobes *IEEE Trans. Nanotechnol.* **5** 50–61
Yin J, Cai W, Zheng Y and Zhao L 2005 Effect of Pt film thickness of PtSi formation and film surface morphology *Surf. Coat. Technol.* **198** 329–34
Zhang L, Bain J A and Zhu J G 2002 Dependence of themal-magnetic mark size on applied STM voltage in Co/Pt multilayers *IEEE Trans. Magn.* **38** 1895–7
Zhang Z, Hellstrom P E, Lu J, Ostling M and Zhang S L 2006 A novel self-aligned process for platinum silicide nanowires *Microelectron. Eng.* **83** 2107–11
Zhuravlev M Y, Sabirianov R F, Jaswal S S and Tsymbal E Y 2005 Giant electroresistance in ferroelectric tunnel junctions *Phys. Rev. Lett.* **94** 246802
Z-TETRAOL Data Sheet Solvay Solexis Inc. 2002 Thorofare, NJ